



UNIVERSITÀ
DEGLI STUDI
DI PADOVA

UNIVERSITA' DEGLI STUDI DI PADOVA

Dipartimento di Ingegneria Industriale DII

Corso di Laurea Magistrale in Ingegneria Meccanica

Validation of the flow profile in a channel facility

Prof. Giorgio Pavesi

Oliver Bortolotti 1106819

Anno Accademico 2015/2016

ABSTRACT

A numerical and experimental investigation in order to discover the velocity profile for a turbulent compressible flow in a channel facility was undertaken. The numerical results were validated by comparison with experimental data and various tests have been taken at subsonic values of Mach number.

For simulating conditions, the governing equations were solved iteratively by using ANSYS CFX 14.0. For turbulent flow simulation, SST k-w model were employed to simulate turbulence.

For experimental conditions, it was used a three hole probe and implementing a code in LabVIEW the instrument has been controlled and the data collected. The channel flow facility is situated in the Turbomachinery's Laboratory at the University of Duisburg-Essen.

Contents

- 1 Introduction** 1

- 2 Numerical Method** 4
 - 2.1 Governing Equations 4
 - 2.2 Turbulence Model 6
 - 2.3 Numerical Procedure 9

- 3 Numerical Results** 14
 - 3.1 Numerical Settings 14
 - 3.2 Non Axial Velocity Components. 15
 - 3.3 Streamline curvature behavior. 16
 - 3.4 Adverse Pressure Gradient Effects. 17

- 4 Experimental Method** 19
 - 4.1 Three hole probe properties and calibration 19
 - 4.2 Experimental Procedure 23
 - 4.3 LabVIEW Code 24

- 5 Experimental Results** 25
 - 5.1 Experimental Setup 25
 - 5.2 Flow angle results 27

6 Validation of the Results 31

6.1 Validation assessment process 31

6.2 Flow validation and discussion 33

7 Possible Solutions to uniform the flow 36

7.1 Changing the Nozzle Geometry 36

7.2 Provide a Honeycomb Structure before the nozzle 39

8 Conclusions 42

9 Appendix A. The LabVIEW “State Machine” Code 43

List of figures

Figure 1.1 Influence of a contraction on variations in the axial velocity distribution

Figure 2.3.1 Geometry of the channel facility.

Figure 2.3.2 Particular of the channel facility.

Figure 2.3.3 Example of a structured grid.

Figure 2.3.4 Geometry model that shows where are applied the boundary conditions.

Figure 2.3.5 Control volume indicating the first data-point from the wall

Figure 3.2.1 Variation in lateral velocity at mid working section on vertical plane (numerical model)

Figure 3.3.1 Streamline curve behavior before the nozzle

Figure 3.4.1 C_p behaviour in the contraction region of the nozzle for Mach number of 0.66

Figure 4.1.1 2-D scheme of the principle parameters involving the three hole probe

Figure 5.1.1 A view of the test section where the probe has been installed.

Figure 5.2.1 Flow angle value plotted for the experimental test with maximum Mach number equal to 0.68.

Figure 6.2.1 Flow angle α value plotted for the numerical and experimental test

Figure 6.2.2 Flow angle γ value plotted for the numerical and experimental test

Figure 7.1.1 Schematic of the contractions (half plane)

Figure 7.1.2 Cp behaviour in the contraction region of the new nozzle geometry for mass flow 1.55 kg/s

Figure 7.2.1 Schematic of several honeycomb cross-sections including square cell, circular cell and regular hexagonal cell.

Figure 7.2.2 Fluid region where honeycomb is installed.

Figure 7.2.3 Variation in lateral velocity at mid working section on vertical plane (new contraction geometry)

List of Tables

Table 3.1 Resume of applied boundary conditions and highest value of Mach number, speed and static pressure drop compared to the ambient pressure in the test section.

Table 5.1 Resume of mass flow at the compressor and highest value of Mach number, speed and static pressure drop compared to the ambient pressure in the test section.

Table 5.2 Flow angle value for the experimental test with maximum Mach number equal to 0.68.

NOTATIONS

Alphabetical conventions

d_h = Hydraulic diameter

F_0 = Total flow area

F_1 = Cross section area

g = Acceleration due to gravity (m/s^2)

M = Mach number

p = Static pressure (Pa)

p_0 = Total pressure (Pa)

p_1 = Pressure inlet nozzle

p_2 = Pressure outlet nozzle

T = Static temperature (K)

u = X-component of velocity (m/s)

u_1 = Velocity inlet nozzle

u_2 = Velocity outlet nozzle

v = Y-component of velocity (m/s)

w = Z- component of velocity (m/s)

z_1 = Height inlet nozzle

z_2 = Height outlet nozzle

Greek conventions

α = Flow angle between u and w (rad)

γ = Flow angle between u and v (rad)

δ = The kronecker delta function

ε = Dissipation

k = Turbulent kinetic energy (J/kg)

λ = Area ratio of the contraction

λ_1 = Friction coefficient of unith honeycomb depth

μ = Fluid viscosity

ρ = Density of the flow (kg/m^3)

1. INTRODUCTION

Duct flow is commonly encountered in engineering. The precise nature of the evolution of turbulent flow through a duct, however, requires further investigation despite over a century of research. The most basic requirements for a rigorous study of fully developed two-dimensional channel flow is clearly a knowledge of the channel dimensions necessary for its establishment. By contrast, there is a distinct scarcity of thorough investigations on the minimum entrance length for fully developed flow- probably due to the many challenges such a study encounters.

In this particular case, a contraction must be also considered. The characteristic geometrical feature of a contraction is the reduction of cross-sectional area with distance along the flow axis. By virtue of the area distribution within a contraction, it follows immediately from the continuity principle that in compressible flow there is a corresponding increase in the mean velocity as the flow passes through the contraction. The mechanical energy equation (equation 1.1) shows that there is a consequent fall in the piezometric pressure.

$$p_1 + \frac{1}{2}\rho U_1^2 + \rho g z_1 = p_2 + \frac{1}{2}\rho U_2^2 + \rho g z_2 + E_d \quad (1.1)$$

A second feature of contractions is their ability to reduce local non-uniformities in the axial velocity profile at a cross-section. Consider a compressible fluid with the axial velocity distribution shown in Fig. 1.1.

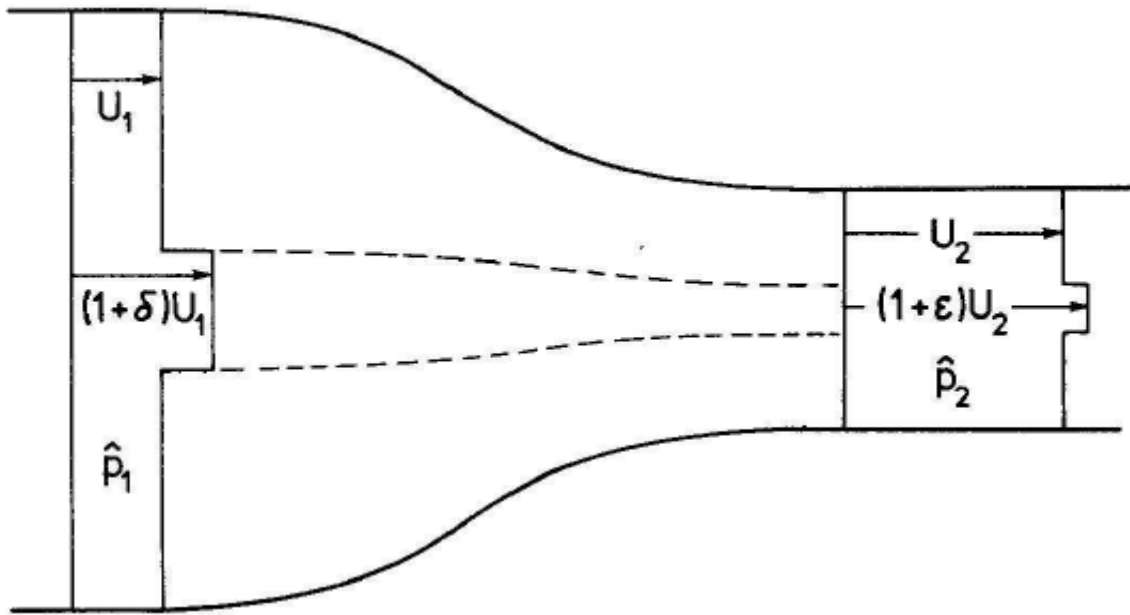


Figure 1.1 Influence of a contraction on variations in the axial velocity distribution.

Approaching the contraction the velocity distribution is uniform except for a small region of increased velocity as shown. The pressure p_1 and p_2 will be assumed uniform over the cross-section. Assuming the flow to be inviscid, the total pressure along any streamtube will be conserved. Hence, in the main field of the flow

$$p_1 + \frac{1}{2}\rho U_1^2 = p_2 + \frac{1}{2}\rho U_2^2 \quad (1.2)$$

And in the high-velocity region

$$p_1 + \frac{1}{2}\rho U_1^2(1 + \delta)^2 = p_2 + \frac{1}{2}\rho U_2^2(1 + \epsilon)^2 \quad (1.3)$$

If the second order effect of the additional mass flow in the small, high velocity region is ignored then from the continuity relation

$$\frac{U_1}{U_2} = \lambda \quad (1.4)$$

Where λ is the area ration of the contraction (having a magnitude in the range $0 < \lambda < 1$). Assuming both δ and ε are small compared with unity, equations (1.2)-(1.4) are easily solved to yield

$$\varepsilon = \lambda^2 \delta \quad (1.5)$$

Showing that the contraction reduces the relative velocity variation by the factor δ^2 , which is the square of the area ratio. Generally to design of a channel facility, the contraction portion should not adverse pressure gradient in the streamwise and further the effect of adverse pressure gradient at the exit of the contraction must be minimal.

The importance to obtain a uniform velocity profile is given by the fact that the entrance region is immediately followed by a diffuser that conduits the air to the compressor.

Diffusers possess fundamental flow characteristics: one of this is the tendency for non-uniformities in the velocity distribution at entry to be maintained or even to be progressively magnified as the flow passes through the diffuser. In particular, the performance of a diffuser is seriously compromised if the flow separates. Regions of stalled flow in a diffuser block the flow, cause low pressure recovery, increasing the loss coefficient.

There are only a limited number of boundary conditions for which exact analytical solutions of the Navier-Stokes equations have been given. The entrance region represents one of those boundary conditions for which such solutions are not available. In addition, published results concerning the longitudinal extension of this development region are rather confusing. This is why it was undertaken this study with the aim of finding out which is the velocity profile of the flow before the diffuser.

2. NUMERICAL METHOD

2.1 GOVERNING EQUATIONS

Computational fluid dynamics or CFD is the analysis of systems involving fluid flow, heat transfer and associated phenomena such as chemical reactions by means of computer-based simulation. CFD codes are structured around the numerical algorithms that can tackle fluid flow problems. In outline the numerical algorithm consists of the following steps:

- Integration of the governing equations of fluid flow over all the (finite) control volumes of the domain
- Discretisation – conversion of the resulting integral equations into a system of algebraic equations
- Solution of the algebraic equations by an iterative method

The motion of a fluid in three dimensions is described by a system of five partial differential equations: mass conservation, x-, y- and z-momentum equations and energy equation.

Equation (2.1.1) is the unsteady, three-dimensional mass conservation or continuity equation at a point in a compressible fluid:

$$\frac{\delta\rho}{\delta t} + \frac{\delta(\rho u)}{\delta x} + \frac{\delta(\rho v)}{\delta y} + \frac{\delta(\rho w)}{\delta z} = 0 \quad (2.1.1)$$

The x-component of the momentum equation is found by setting the rate of change of x-momentum of the fluid particle equal to the total force in the x-direction on the element due to surface stresses plus the rate of increase of x-momentum due to sources. Considering a Newtonian fluid, where the viscous stresses are proportional to the rates of deformation, the result is

$$\frac{\delta(\rho u)}{\delta t} + \text{div}(\rho u \mathbf{u}) = -\frac{\delta p}{\delta x} + \text{div}(\mu \text{grad } u) + S_{Mx} \quad (2.1.2)$$

The y- and z- component of the momentum equation are found with the same method

$$\frac{\delta(\rho v)}{\delta t} + \text{div}(\rho v \mathbf{u}) = -\frac{\delta p}{\delta y} + \text{div}(\mu \text{grad } v) + S_{My} \quad (2.1.3)$$

$$\frac{\delta(\rho w)}{\delta t} + \text{div}(\rho w \mathbf{u}) = -\frac{\delta p}{\delta z} + \text{div}(\mu \text{grad } w) + S_{Mz} \quad (2.1.4)$$

The energy equation is derived from the first law of thermodynamics, which states that the rate of change of energy of a fluid particle is equal to the rate of heat addition to the fluid particle plus the rate of work done on the particle. As before, we define a source of energy S_E per unit volume per unit time. The energy equation is

$$\begin{aligned} \rho \frac{DE}{Dt} = & -\text{div}(\rho u) \\ & + \text{div}(k \text{grad } T) \left[\frac{\delta(u\tau_{xx})}{\delta x} + \frac{\delta(u\tau_{xy})}{\delta x} + \frac{\delta(u\tau_{xz})}{\delta z} + \frac{\delta(v\tau_{yx})}{\delta x} + \frac{\delta(v\tau_{yy})}{\delta y} + \frac{\delta(v\tau_{yz})}{\delta z} \right. \\ & \left. + \frac{\delta(w\tau_{wx})}{\delta x} + \frac{\delta(w\tau_{wy})}{\delta y} + \frac{\delta(w\tau_{ww})}{\delta z} \right] + S_E \quad (2.1.5) \end{aligned}$$

In equation (2.1.5) we have $E = i + \frac{1}{2} * (u^2 + v^2 + w^2)$.

This system of equations governs every turbulent flow, but we investigate the effects of fluctuations on the mean flow using the Reynolds decomposition, replacing the flow variables u,v, w and p by the sum of a mean and fluctuating component. Thus

$$\mathbf{u} = \mathbf{U} + \mathbf{u}' \quad u = U + u' \quad v = V + v' \quad w = W + w' \quad p = P + p'$$

Considering the continuity equation, first we note that $\text{div } u = \text{div } \mathbf{U}$. This yields the continuity equation for the mean flow $\text{div } \mathbf{U} = 0$. Substitution of this and a similar process on the x-,y-

and z- momentum equations let to find the so called Reynolds averaged Navier Stokes equations (RANS equations) (Eqn. 2.1.6-2.1.8)

$$\frac{\delta U}{\delta t} + \text{div}(UU) = -\frac{1}{\rho} \frac{\delta p}{\delta x} + \nu \text{div}(\text{grad}(U)) + \frac{1}{\rho} * \left[\frac{\delta(-\rho u'^2)}{\delta x} + \frac{\delta(-\rho u'v')}{\delta y} + \frac{\delta(-\rho u'w')}{\delta z} \right]$$

$$\frac{\delta V}{\delta t} + \text{div}(VU) = -\frac{1}{\rho} \frac{\delta p}{\delta y} + \nu \text{div}(\text{grad}(V)) + \frac{1}{\rho} * \left[\frac{\delta(-\rho u'v')}{\delta x} + \frac{\delta(-\rho v'^2)}{\delta y} + \frac{\delta(-\rho v'w')}{\delta z} \right]$$

$$\frac{\delta W}{\delta t} + \text{div}(WU) = -\frac{1}{\rho} \frac{\delta p}{\delta z} + \nu \text{div}(\text{grad}(W)) + \frac{1}{\rho} * \left[\frac{\delta(-\rho u'w')}{\delta x} + \frac{\delta(-\rho v'w')}{\delta y} + \frac{\delta(-\rho w'^2)}{\delta z} \right]$$

2.2 TURBULENCE MODEL

Flows in the laminar regime are completely described by the RANS equations. Many, if not most, flows of engineering significance are turbulent. Fluid engineers need access to viable tools capable of representing the effects of turbulence. In order to be able to compute turbulent flow with the RANS equations it is necessary to develop turbulence models to predict the Reynolds stresses and the scalar transport terms and close the system of mean flow equations. The most common RANS turbulence models are classified on the basis of the number of additional transports equations that need to be solved along with the RANS flow equations.

The k-ε model is well established and widely used. It is derived for high Reynolds number flow and the coefficients are empirically derived. For this model the transport equations are kinetic turbulent energy, k , which is defined as,

$$k = \frac{1}{2} * (u'_i u'_j) \quad (2.2.1)$$

and the dissipation of turbulent kinetic energy, ε, which is defined as,

$$\varepsilon = \nu * \frac{\delta u'_i}{\delta x_j} * \frac{\delta u'_i}{\delta x_j} \quad (2.2.2)$$

The final equation for these two transport properties, k and ε , takes the following final form as expressed in equation (2.2.3) and equation (2.2.4) respectively

$$\frac{\delta k}{\delta t} + \frac{u_j(\delta k)}{\delta x_j} = \nu_t * \left(\frac{\delta u_i}{\delta x_j} + \frac{\delta u_j}{\delta x_i} \right) * \frac{\delta u_i}{\delta x_j} + \frac{\delta}{\delta x_j} \left[\frac{\left(\nu + \frac{\nu_t}{\sigma_k} \right) \delta k}{\delta x_j} \right] - \varepsilon \quad (2.2.3)$$

$$\frac{D\varepsilon}{Dt} = C_{\varepsilon 1} * \frac{\varepsilon}{k} (-u'_i u'_j) * \frac{\delta u_i}{\delta x_j} + \frac{\delta}{\delta x_j} * \left[\left(\nu + \frac{\nu_t}{\sigma_\varepsilon} \right) * \frac{\delta \varepsilon}{\delta x_j} \right] - C_{\varepsilon 2} * \frac{\varepsilon^2}{k} \quad (2.2.4)$$

The model constants are $C_{\varepsilon 1} = 1.44$, $C_{\varepsilon 2} = 1.92$, $\sigma_k = 1.0$, $\sigma_\varepsilon = 1.3$.

The rate of dissipation of turbulence kinetic energy ε is not the only possible length scale determining variable. The most prominent alternative is the k- ω model proposed by Wilcox, The K-omega model is one of the most commonly used turbulence models. It is a two equation model, that means, it includes two extra transport equations to represent the turbulent properties of the flow. This allows a two equation model to account for history effects like convection and diffusion of turbulent energy. The first transported variable is turbulent kinetic energy, k. The second transported variable in this case is the specific dissipation, ω . It is the variable that determines the scale of the turbulence, whereas the first variable, k, determines the energy in the turbulence.

Mentor noted that the results of the k- ε model are much less sensitive to the assumed values in the free stream, but its near-wall performance is unsatisfactory for boundary layers with adverse pressure gradients. This led him to suggest a hybrid model using a transformation of the k- ε model into a k- ω model in the near-wall region and the standard k- ε model in the fully turbulent region far from the wall. The SST k- ω turbulence model is a

two-equation eddy-viscosity model which has become very popular. The shear stress transport (SST) formulation combines the best of two worlds. The use of a k- ω formulation in the inner parts of the boundary layer makes the model directly usable all the way down to the wall through the viscous sub-layer, hence the SST k- ω model can be used as a Low-Re turbulence model without any extra damping functions. The SST formulation also switches to a k- ϵ behavior in the free-stream and thereby avoids the common k- ω problem that the model is too sensitive to the inlet free-stream turbulence properties. Authors who use the SST k- ω model often merit it for its good behavior in adverse pressure gradients and separating flow. The SST k- ω model does produce a bit too large turbulence levels in regions with large normal strain, like stagnation regions and regions with strong acceleration. This tendency is much less pronounced than with a normal k- ϵ model though.

$$\frac{\delta k}{\delta t} + U_j * \frac{\delta k}{\delta x_j} = P_k - \beta^* k \omega + \frac{\delta}{\delta x_j} \left[(v + \sigma_k v_T) * \frac{\delta k}{\delta x_j} \right] \quad (2.2.5)$$

$$\frac{\delta \omega}{\delta t} + U_j * \frac{\delta \omega}{\delta x_j} = \alpha S^2 - \beta \omega^2 + \frac{\delta}{\delta x_j} \left[(v + \sigma_w v_T) * \frac{\delta \omega}{\delta x_j} \right] + 2(1 - F_1) \sigma_{w2} * \frac{1}{\omega} * \frac{\delta k}{\delta x_i} * \frac{\delta \omega}{\delta x_i} \quad (2.2.6)$$

The model constants are $\beta^* = \frac{9}{100}$, $\sigma_{k1} = 0.85$, $\sigma_{k2} = 1$, $\sigma_{w1} = 0.5$, $\sigma_{w2} = 0.856$

2.3 NUMERICAL PROCEDURE

The three-dimensional model of the channel facility was done by using ICEM CFD 14.0.

The geometry is showed in figure 2.3.1.

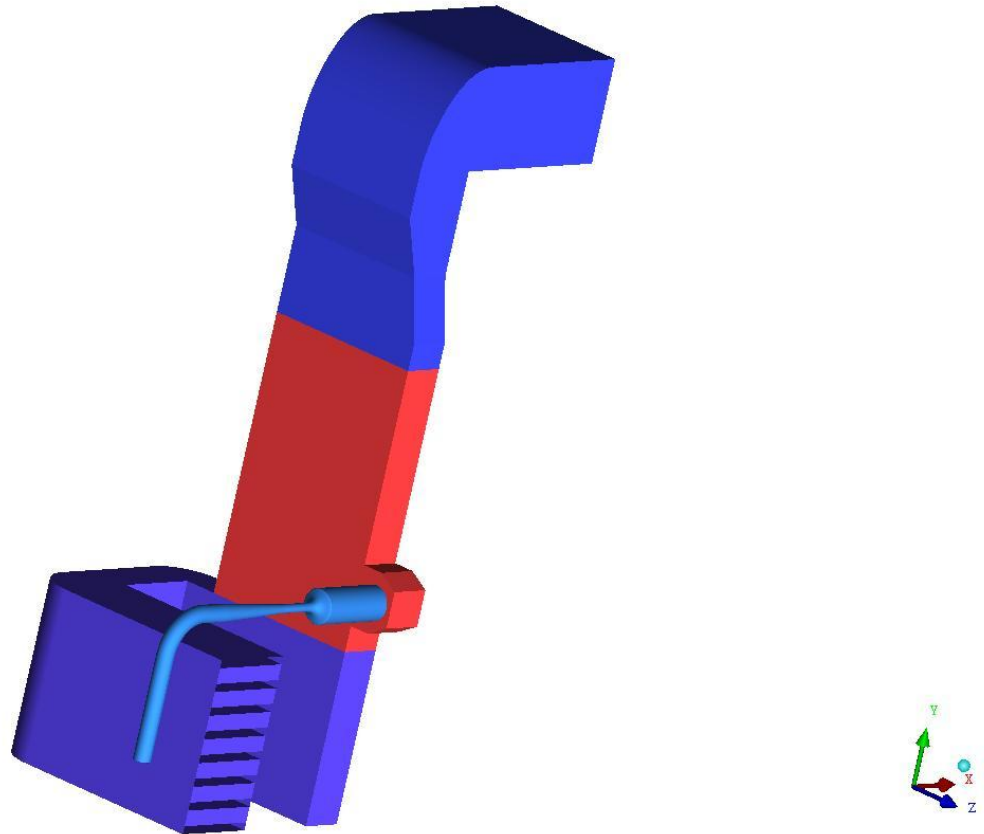
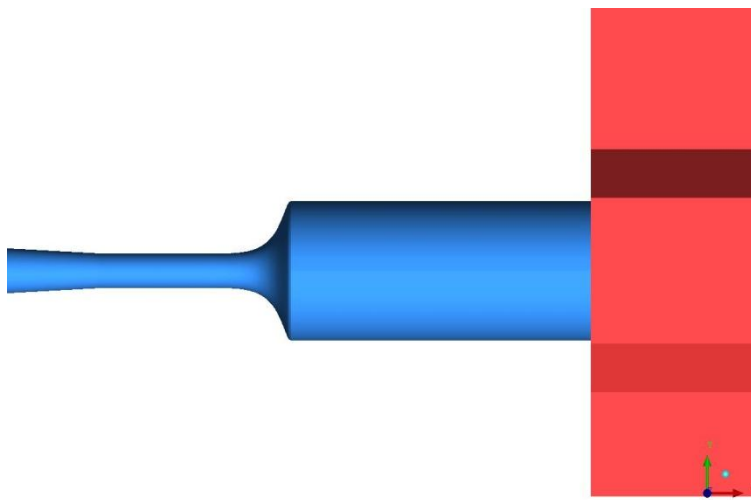


Figure 2.3.1 Geometry of the channel facility.

The air enters the duct through a chimney located on the upper floor of the building, goes through a rectangular cross-section pipe (the red one) and here is divided by a T-junctions. Therefore, there are two outlets, one goes to the radial compressor (not showed in figure) located after the diffuser and the bend, the other conducts the flow to an area located downstairs in the building. At the second outlet, seven separated blocks are placed as silencer function. Some parts of the models contains uncertainties regarding the geometry. For example, the rectangular cross section pipe leading to the T-junction and parts of the

geometry of the T- junction itself are supposed because they were surrounded by the wall and incomplete data were available about them.



Focusing the attention on the first division (figure 2.3.2), the model was a constant cross-section circular conduit. The length and the diameter of the first circular conduit were 1 m and 0.4 m, respectively. After it, a nozzle was located reducing the diameter to a value of 0.1 m and length 0.151m.

Figure 2.3.2 Particular of the channel facility.

Afterwards, before the diffuser, it is located a second circular conduit length 0.43 m. The test section is located in the pipe between the nozzle and the diffuser.

In order to numerically solve the governing momentum, energy and turbulence equations for CFD simulations, it is necessary to discretized or partition a normally continuous region into distinct volumetric cells. All of the volumetric cells collectively make up the simulation's computational domain.

The mesh was done by using ICEM CFD 14.0. The type of mesh used was structured grids. Structured grids are characterized by regular connectivity that can be expressed by a two or three dimensional array which decreases the storage requirement and makes for efficient solver algorithms. Structured grids are restricted to quadrilateral elements in the surface mesh and hexahedral elements in the volume, an example of a structured grid is shown in Figure 2.3.3. A well designed structured grid gives a solution of high accuracy, however the process of generating such a grid is a tedious task.

Unstructured grids are avoided because they could compromise the solution. The elements have no particular ordering and are placed in an irregular fashion, therefore the solution is approximated. For this reason the type of mesh used was structured grids.

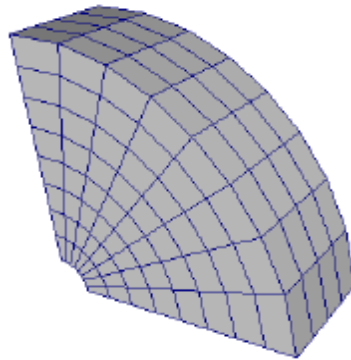


Figure 2.3.3 Example of a structured grid.

The air inlet was assumed to be uniform flow. As inlet boundary condition, it has fixed that the pressure static is equal to the pressure ambient. At the wall, no-slip boundary condition was applied.

The numerical scheme for pressure and momentum was high resolution. To improve the convergence of the solution, a first solution was carried out using Upwind numerical scheme, then another simulation with high resolution as numerical scheme was launched using as initial solutions the results of the Upwind scheme.

Some grid refinement tests have been done on the flow fields of circular conduit to obtain grid independent solution. This was obtained assuring that the lowest angle of the mesh was 25° , quality higher than 0.4, aspect ratio and volume change respectively lower than 80 and 20. At the end the mesh contained about 5 million nodes.

The numerical solution was carried out with the maximum residual less than 10^{-4} .

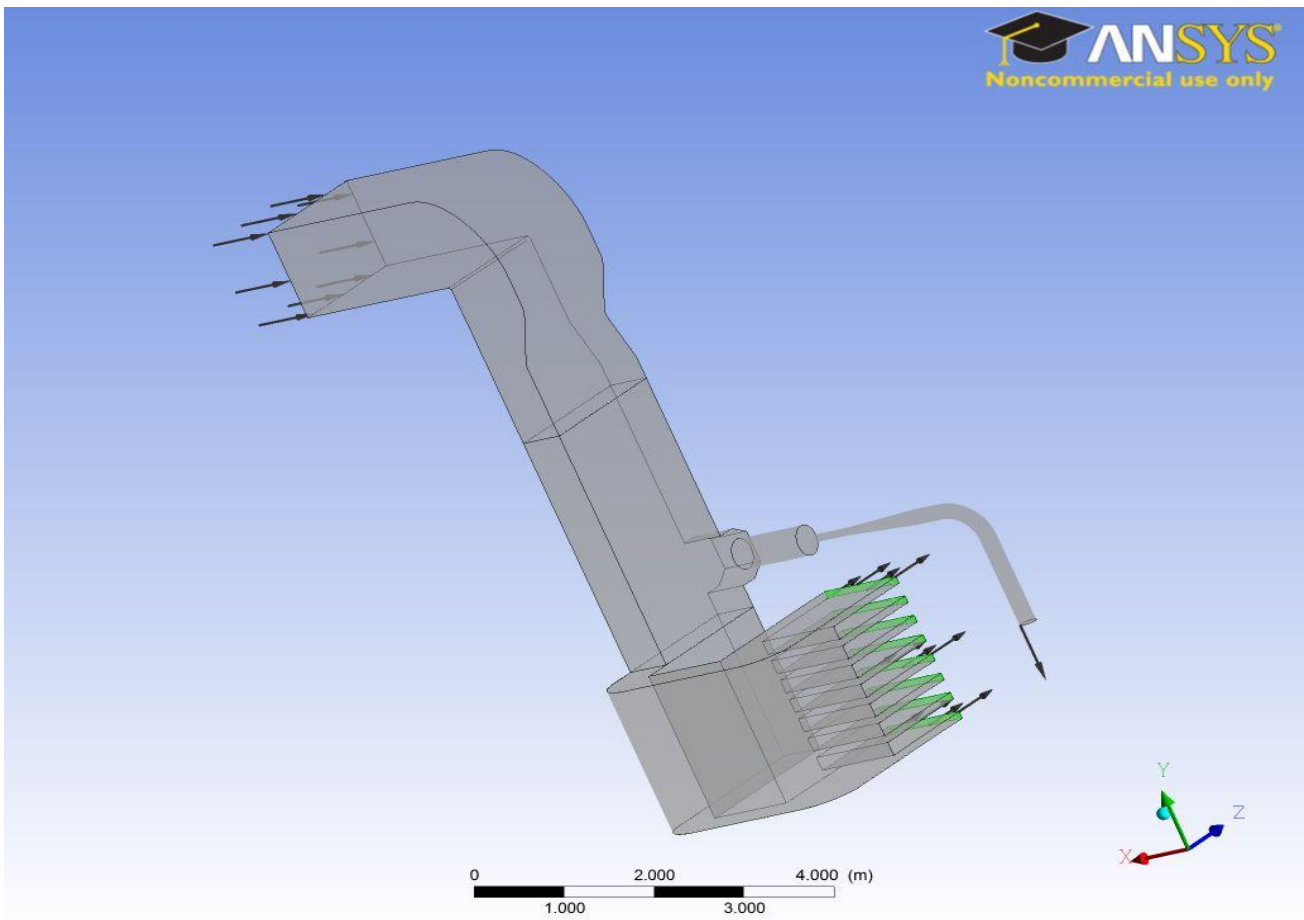


Figure 2.3.4 The figure shows where are applied the boundary conditions.

Regarding the turbulence model and the wall y^+ strategy, turbulent flows are significantly affected by the presence of walls, where the viscosity regions have large gradients in the solution variables. It can be observed that the viscosity-affected region is made up of three zones, namely the:

- Viscous sublayer ($y^+ < 5$)
- Buffer layer ($5 < y^+ < 30$)
- Log-law region ($y^+ > 30$)

The wall coordinate, y^+ , is a dimensionless parameter and it is an accurate way of determining the distance from the wall to the nearest data-point in the mesh. As the flow

solution is computed on the cell center, this means that the first data-point from the wall will be in the middle of the first cell as Figure 2.3.5 indicates

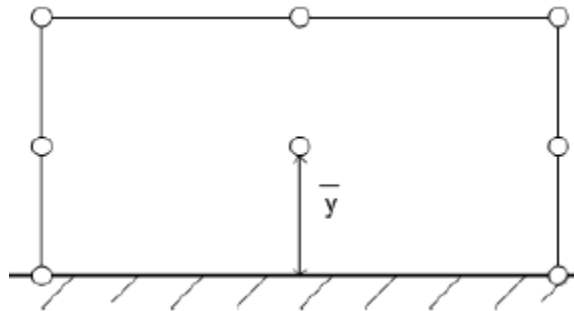


Figure 2.3.5 Control volume indicating the first data-point from the wall

The y^+ regions serves as an indicator on how fine the mesh has to be to achieve accurate calculations. For the purpose of this study, a wall y^+ in the range of 30 is determined to be sufficiently accurate.

The $k-\omega$ SST by Menter is chosen to model the turbulence. The $k-\omega$ model is known for its abilities to accurately predict the turbulence close to the wall, all the way down to the viscous sub-layer and to correctly predict separation zones. The downside of the $k-\omega$ model is that it is heavily influenced by the turbulence boundary conditions in the free-stream zone far away from the wall. The $k-\epsilon$ model is relatively insensitive to these boundary conditions and provides a more accurate view of the turbulence development in the area far away from the wall. The $k-\omega$ SST model combines the best of both worlds by switching and averaging between the $k-\epsilon$ and the $k-\omega$ models depending on the distance from the wall.

3. NUMERICAL RESULTS

3.1 NUMERICAL SETTINGS

For this geometry, two runs have been systematically performed with outlet conditions at the radial compressor mass flow rate set to 1.55 and 1.45 kg/s respectively. At the second outlet, a velocity normal to boundary condition equal to 4m/s. This value has been measured using an anemometer during the tests. As inlet boundary condition, the pressure static has been set to 1 atmosphere, assumed a uniform mean longitudinal velocity distribution.

The results shown in table 3.1 report the set boundary conditions, the highest value of Mach number, speed and maximum static pressure drop compared to the ambient pressure in the test section.

| INLET [atm] | OUTLET 1 [kg/s] | OUTLET 2 [m/s] | Max Mach number test section | Max speed test section [m/s] | Max pressure drop test section [Pa] |
|-------------|-----------------|----------------|------------------------------|------------------------------|-------------------------------------|
| 1 | 1.55 | 4 | 0.66 | 209.66 | -26410 |
| 1 | 1.45 | 4 | 0.57 | 190.66 | -21644.9 |

Table 3.1 Resume of applied boundary conditions and highest value of Mach number, speed and static pressure drop compared to the ambient pressure in the test section

Referring to the table, the velocity u is the axial velocity, the velocity v and w are the two normal velocities at the axis of the pipe.

3.2 NON AXIAL VELOCITY COMPONENTS

The uniformity of the flow was compared at the mid working section immediately after the nozzle. The velocities component along the y and z axis for the value of Mach number 0.66 are shown in Figure 3.2.1. Referring to the model, the velocity u is the axial velocity, the velocity v and w are the two normal velocities at the axis of the pipe. This result demonstrated not reasonably uniform flow across the wind tunnel middle plane.

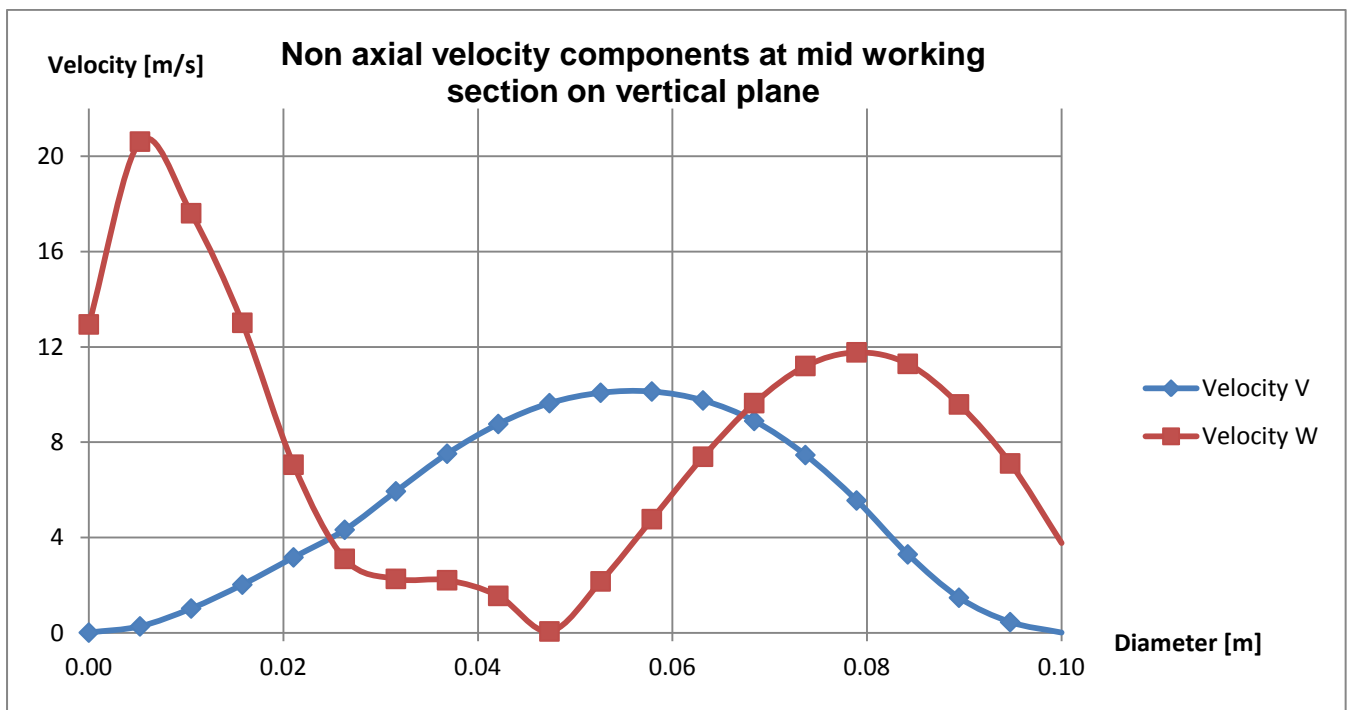


Figure 3.2.1 Variation in lateral velocity at mid working section on vertical plane

The velocity along the y- and z- axis achieved important values. Compared to the axial velocity, that in this case is about 210 m/s, those values cannot be neglect.

The results for Mach number equal to 0.57 showed quite the same behavior.

3.3 STREAMLINE CURVE BEHAVIOR

The initial Non-uniformity has an important effect on the behavior of the flow after the nozzle. The flow through 90° pipe bends is characterized by flow separation, secondary flow and unsteadiness, which are dependent on Reynolds number. Low free stream turbulence is extremely stringent for subsonic wind tunnel and it also affects the flow quality.

This is clear plotting the streamlines curve (figure 3.3.1), that show the direction in which a massless fluid element will travel at any point in time.

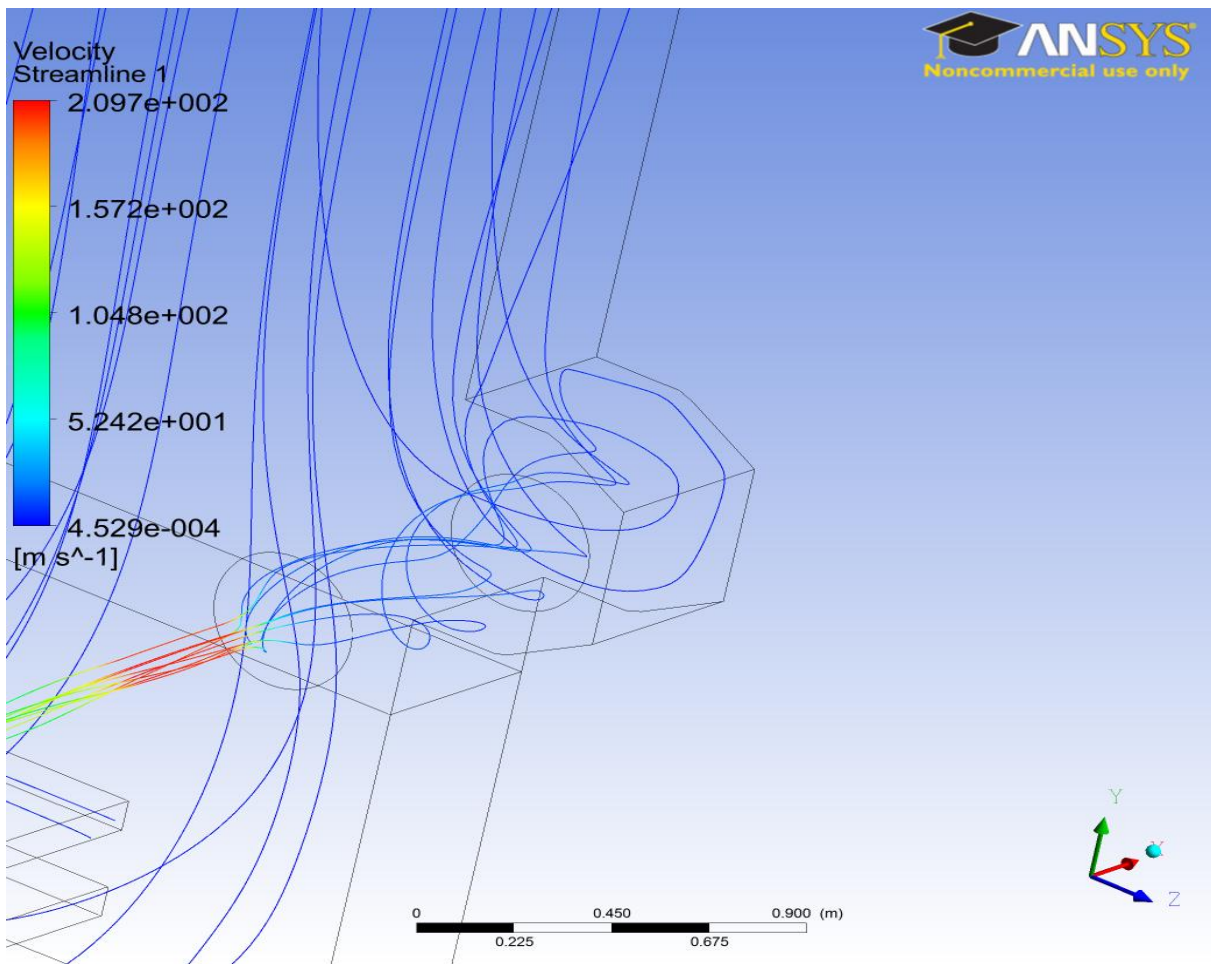


Figure 3.3.1 Streamline curve behavior before the nozzle

This is the most important effect that doesn't allow the flow to be uniform after the nozzle. Hence for better simulation of experimental conditions, turbulence intensity in the test section should be minimized and velocity profile in the test section should be maintained as uniform as possible. A solution is showed in the following chapters.

3.4 ADVERSURE PRESSURE GRADIENT EFFECTS

Whenever a converging duct segment is attached to a constant-area, regions of adverse pressure gradients will occur along the wall, at its inlet and exit that may cause boundary layer separation. If separation occurs, it will degrade the flow uniformity and steadiness, both of which are essential in a test facility.

This phenomenon occurred at the outlet of the contraction because the wall changes suddenly from a curved to a flat region, thus the streamline near the wall would accumulate and eventually increase the relative pressure in this region. Theoretically, to delay separation, it is better that a longer contraction's length be chosen, but this will increase the cost and thickening the boundary layer that may enhance boundary layer and risk of separation. Furthermore, if the length is reduced, the contraction costs will reduce and it will fit into a smaller space. Thus the length must be optimized. The contraction area ratio is another dominant factor that affects the extent of flow uniformity, flow separation and downstream turbulence level.

The general aerodynamic performance of the contraction is given by the static pressure distribution, C_p , along the wall

$$C_p = \frac{P - P_\infty}{\frac{1}{2} * \rho * U_\infty^2} \quad (3.4.1)$$

Where P is the static pressure measured along the wall, P_∞ and U_∞ is the static pressure and the mean velocity measured at the outlet of the contraction, respectively. Fig. 3.4.1 shows the measured static pressure distribution in the contraction region of the nozzle at Mach number=0.66. This plot indicates that the distribution is smooth and favorable except for the exit regions of the nozzle. That will cause an accumulation of the streamline near the wall and eventually increases the relative pressure, adverse pressure gradient, in this region. By increasing the velocity, this adverse pressure gradient strengthens. The unfavorable pressure gradient in this area may be due to the change from a curved wall to a flat surface along the wall. Additionally, the near wall streamline velocity is greater than the axial middle contraction velocity, when the flow arrives to the flat surface, velocity profile like to be uniform and it cause to streamline velocity near the wall decreases and consequently increase in relative pressure (adverse pressure gradient) is happened. In the figure presented below, the inlet position of the nozzle is taken at $x=-0.906$ m and the outlet position is at $x=-1.151$ m.

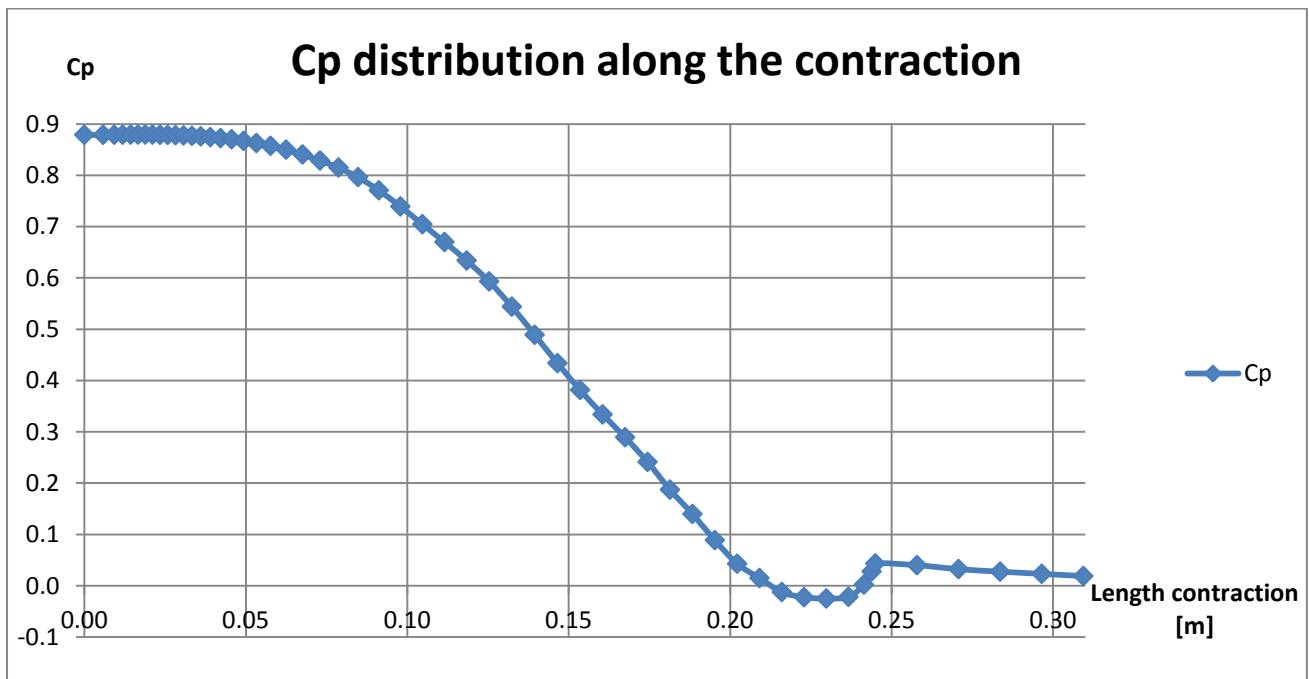


Figure 3.4.1 Cp behaviour in the contraction region of the nozzle for Mach number of 0.66

4. EXPERIMENTAL METHOD

4.1 THREE HOLE PROBE PROPERTIES AND CALIBRATION

The harsh turbomachine environment makes three-hole pressure probes particularly attractive for the measurement of flow pressure, velocity and direction. On the other hand, these types of probes are becoming more useful with the development of small inexpensive fast response pressure transducers, computer controlled traversing systems, and computer based data acquisition and analysis.

Differential pressure measurements provide a useful alternative to hot-wire and hot-film anemometry for determining complex flow directions and even turbulence intensity.

Separate measurements of the total and static pressures can yield both the mean and fluctuating components of velocity and pressure.

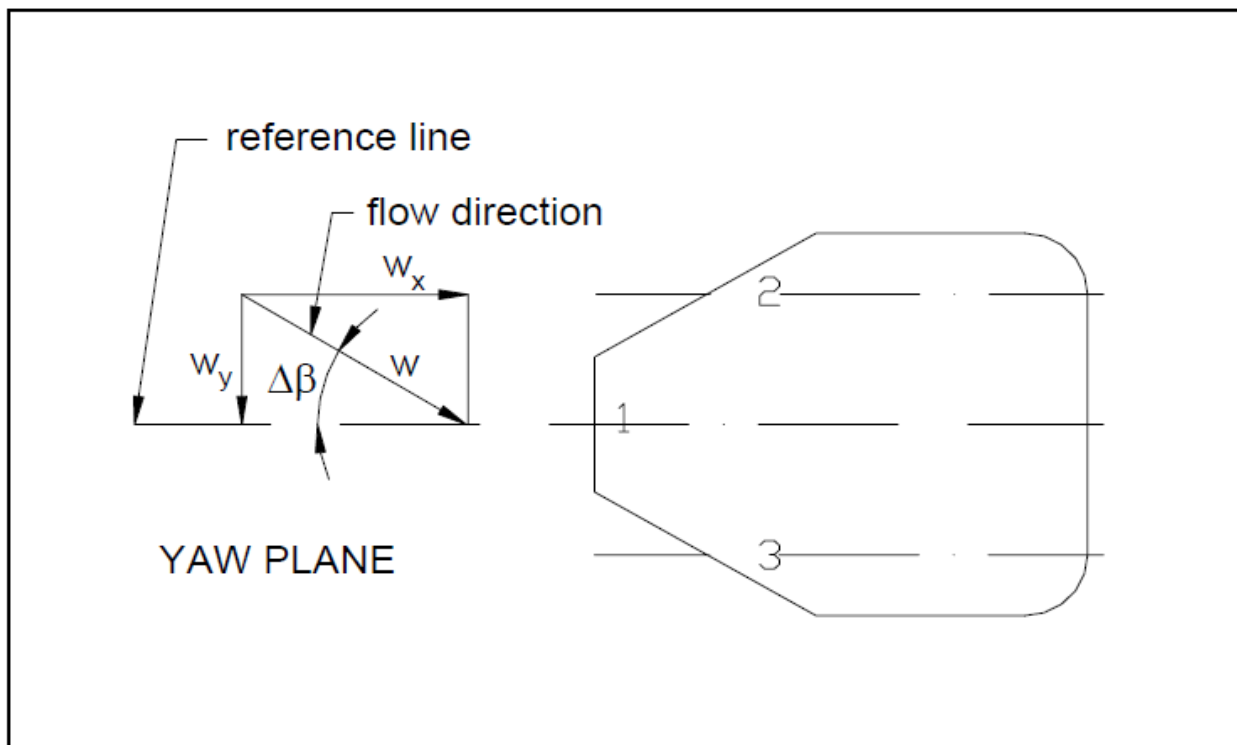


Figure 4.1.1 2-D scheme of the principle parameters involving the three hole probe

The objective of an aerodynamic probe - in the present context - is to determine the scalar and vector properties of complicated flow fields such as those encountered around complex bodies or in turbomachines, in terms of static and total pressure and two-dimensional (2D) velocity components respectively.

The angle between the velocity vector w and the probe axis, over the yaw plane, is the yaw angle $\Delta\beta$. To determine the two-dimensional orientation and magnitude of the flow vector, the surface pressure is sampled at three locations: on the axis of the probe and at two same spaced points on the probe sides. The central pressure tap gives the conventional stagnation pressure when the flow vector is perpendicular to that point on the surface. The pressure difference between the pressure side sensing-holes may be related to the inflow velocity vector by using an appropriate calibration to deduce the yaw direction.

This translates into a measurement of pressures, which by means of calibration functions and gas dynamic relationships, are subsequently converted into flow angles and Mach numbers.

For both, calibration and application, the probe's reference line is defined by some consistent characteristic of the probe's geometry. In application, a reference direction obtained by placing p_2 with p_3 is not always meaningful, since initially a known flow direction would be required to relate the balanced condition to an absolute spatial reference.

The probe can be operated in two ways:

- Nulling technique
- Stationary method (non-nulling technique)

The nulling technique is the most accurate but mechanically complex. It is the most simple in terms of data analysis, as well.

The probe is mounted on a three degree of freedom traversing system and is oriented such that the X-axis is parallel to the flow (yaw and pitch angles are both zero). The center pressure tap measures the stagnation pressure p_1 and the pressures in the two outer tubes are equal ($p_2 = p_3$) and proportional to the static pressure. Finally, the probe position is noted and the flow direction is determined from a calibrated scale.

This nulling technique requires a very sophisticated traversing system and long data acquisition time, since the probe must be yawed at each measurement location until the two pressures are equal. This can take a long time, especially if the probe is small and has a slow time response.

If space limitations or other considerations make nulling techniques impractical, three-hole probes in a non-nulling mode can be employed for measurements in low speed, incompressible flows.

The stationary method or non-nulling technique tends to be less accurate but offers simplicity in installation. The latter characteristic is the most important in turbomachine applications. It is performed by setting the probe at constant pitch and yaw values with respect to the test section. The three pressures are measured at each measurement location by traversing the probe over the flow field. From these three measured pressures, the direction and magnitude of the flow with respect to the X-axis of the pressure probe are determined.

Although elegant in its simplicity, this technique encounters singularity when calibration for large angle of yaw is sought. So it is restricted to lower flow angle ranges, preventing its use in highly 3D flows.

For the steady state, the Bernoulli conservation equation for energy is:

$$p + \rho * \frac{w^2}{2} = \text{const.} \quad (4.1.1)$$

The pressure p in Eq. (4.1.1) is the static pressure. It is the component of the pressure that represents fluid hydrostatic effects. And in principle, it is measured by an instrument that moves along with the fluid. This is, however, inconvenient, and the pressure is usually measured via a small hole in a wall arranged so that it does not disturb the flow. The quantity $\rho * \frac{w^2}{2}$ is usually called dynamic pressure. It is the component of the fluid that represents fluid kinetic energy.

Total pressure p_t , sometimes also called “stagnation pressure”, is defined as the pressure that would be reached if the local flow is imagined to slow down to zero velocity, frictionlessly. Total pressure is the sum of static and dynamic pressure:

$$p_t = p + \rho * \frac{w^2}{2} \quad (4.1.2)$$

From measurements of the total and static pressures, the velocity can be obtained as,

$$w = \sqrt{\left(\frac{2}{\rho}\right) * (p_t - p)} \quad (4.1.3)$$

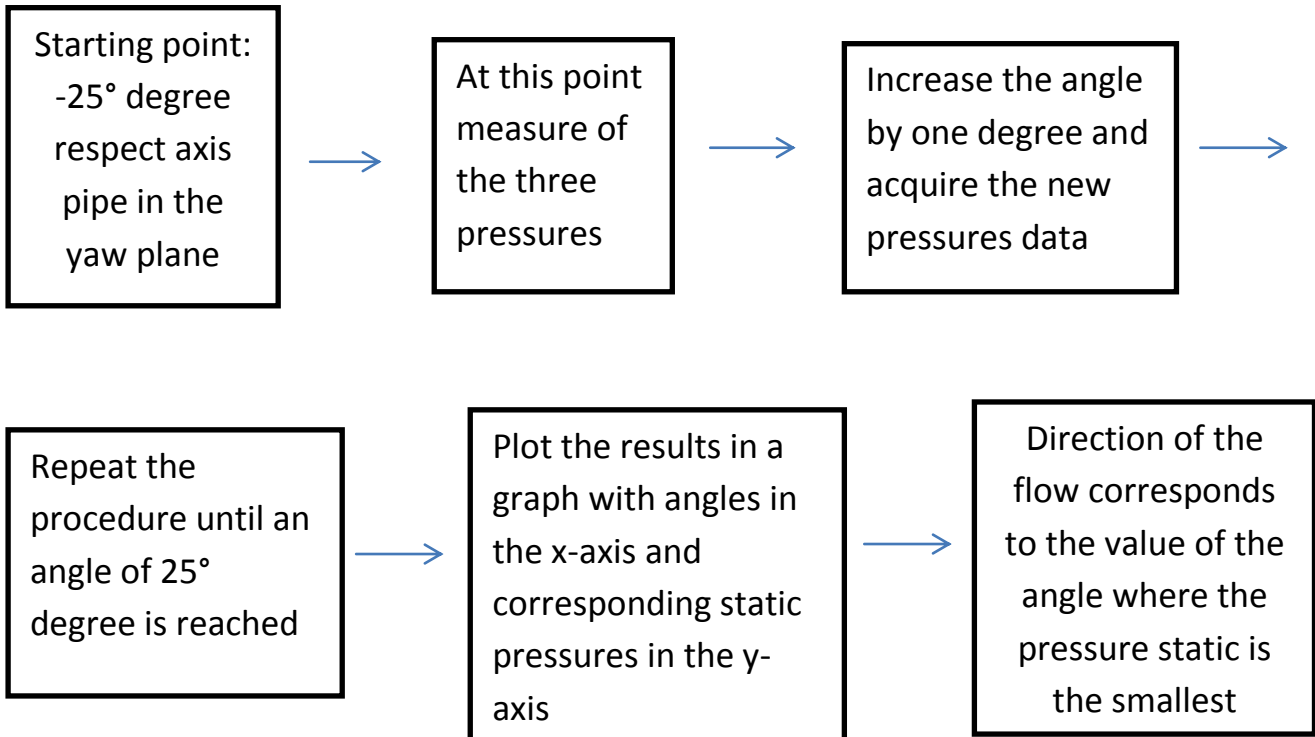
4.2 EXPERIMENTAL PROCEDURE

For data acquisition and instrument control has been used LabVIEW National Instruments program.

The three-hole probe has been connected to an engine allowing the instrument to translate and rotate during the measure acquisition.

The code to connect the computer to the engine and command its launch, movement and direction using the keyboard was already implemented by the researchers of the university.

The work that has been done was to automatize the procedure of calibration the probe. The philosophy that has been chosen was to use the stationary method or non-nulling technique: the initial position of the probe was set to an angle sloped -25° degrees to the axis of the pipe in the yaw plane. At this point a first measure of the pressures has been taken. Successively we enter a loop, where the angle is increased by one degree and every cycle the pressures data have been collected. This is done until the position of the probe has reached 25° degrees. According to the theory, the direction and magnitude of the flow has been found where the value of the pressure static is the smallest.



4.3 LABVIEW CODE

One tool that has been used by programmers in order to automatize and obtain a faster and easier way to develop software is the *state machine*.

State machines allow the program to change the way it executes based on inputs and results of the application. It revolves around three concepts: the state, the event and the action. States describe the status of a piece of programming and are subject to change over time. Events are occurrences in time that have significant meaning to the piece of code controlled by the state machine. This external occurrence will inform the state machine that the correct event has occurred and a transition from states is now appropriate. Actions are response to events. The state machine determines which action needs to be taken when a given event occurs. This decision of what action needs to be taken is derived from two pieces of information: the current state and the event that has occurred.

A state machine, in simple terms, is a case structure inside a While loop. The While loop provides the ability to continuously execute until the conditional operator is set “true”. The case statements allows for variations in the code to be run.

The style that has been used for the state machine is the sequence style. This version is used when the order of execution of the tasks to be performed is predefined, and it will always execute from beginning to end in order. In this type of systems, there are a number of distinct steps that need to be performed in a defined order. These steps can be used to create the states in the state machine.

5. EXPERIMENTAL RESULTS

5.1 EXPERIMENTAL SETUP

A single component three hole probe was used to investigate the flow uniformity in the test section.

In the test section, the probe was placed on a stand facing the flow coming from the contraction exit as shown in figure 5.1.1. By traversing the probe, measurements were taken in one cross-sectional plane, located 250 mm from the contraction exit. The measurements were taken at 20 equally spaced locations, separated by 5 mm. The upper and lower translation value distance 2-3 mm from the wall.

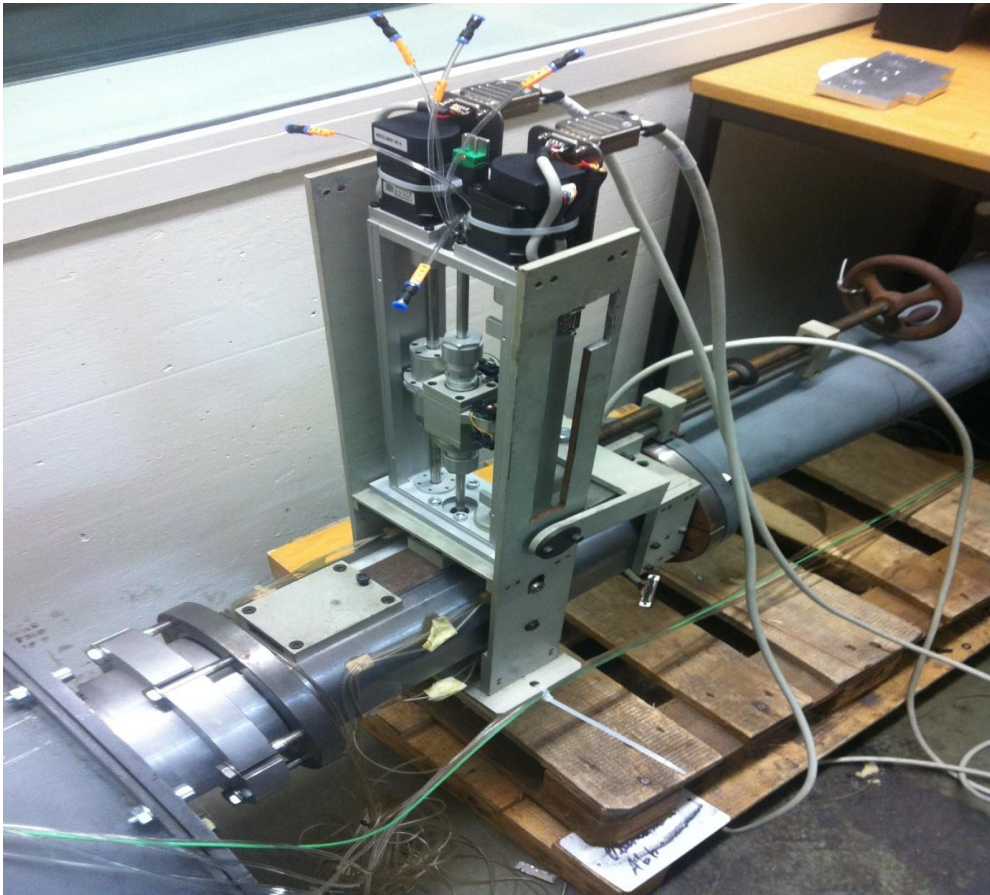


Figure 5.1.1 A view of the test section where the probe has been installed.

As said before, an engine controlled by the program developed in LabVIEW allows the probe to move in translation and rotational directions. To reduce the uncertainty, for every space locations more measurements have been taken. The results in the next chapter show the mean value.

To validate the numerical results, the conditions with mass flow rate passing through the test section of 1.45 and 1.55 kg/s were tested and to control the mass flow passing through the pipe, the revolutions per minute of the compressor were changed. Then the results were written in a text file.

The results shown in table 5.1 report the mass flow at the compressor, the highest value of Mach number, speed and maximum static pressure drop compared to the ambient pressure in the test section.

| Mass flow at the compressor [kg/s] | Max Mach number test section | Max speed test section [m/s] | Max pressure drop test section [Pa] |
|------------------------------------|------------------------------|------------------------------|-------------------------------------|
| 1.55 | 0.68 | 218.40 | -27342 |
| 1.45 | 0.58 | 194.48 | -21396 |

Table 5.1 Resume of mass flow at the compressor and highest value of Mach number, speed and static pressure drop compared to the ambient pressure in the test section

5.2 FLOW ANGLE VALUES

In the experimental results the uniformity of the flow was compared using the value of the flow angles. For this reason two new parameters have been introduced:

$$\alpha = \text{atan}\left(\frac{w}{u}\right) \quad (5.2.1)$$

$$\gamma = \text{atan}\left(\frac{v}{u}\right) \quad (5.2.2)$$

As said, the measurements were taken at 20 space locations in the test section, separated by 5 mm. For every translation points, more measurements have been taken and the results show the mean value. The table 5.2 shows the results for the experimental test with Mach number equal to 0.68.

| Translation (from lower to upper point) [mm] | α [rad] | γ [rad] |
|--|----------------|----------------|
| 0 | 6.75 | 1.61 |
| 5 | 5.86 | 2.10 |
| 10 | 4.15 | 2.50 |
| 15 | 2.82 | 2.83 |
| 20 | 1.67 | 2.93 |
| 25 | 0.98 | 3.29 |
| 30 | 0.99 | 3.63 |
| 35 | 0.98 | 3.67 |
| 40 | 0.85 | 3.96 |
| 45 | 0.66 | 4.02 |

| | | |
|----|------|-------|
| 50 | 0.32 | 3.91 |
| 55 | 0.52 | 3.91 |
| 60 | 0.69 | 3.63 |
| 65 | 0.79 | 3.299 |
| 70 | 1.02 | 3.01 |
| 75 | 1.18 | 2.73 |
| 80 | 1.12 | 2.43 |
| 85 | 0.78 | 2.16 |
| 90 | 0.76 | 1.93 |
| 95 | 0.79 | 1.85 |

Table 5.2 Flow angle value for the experimental test with maximum Mach number equal to 0.68.

Plotting the analytical value figure 5.2.1 is obtained:

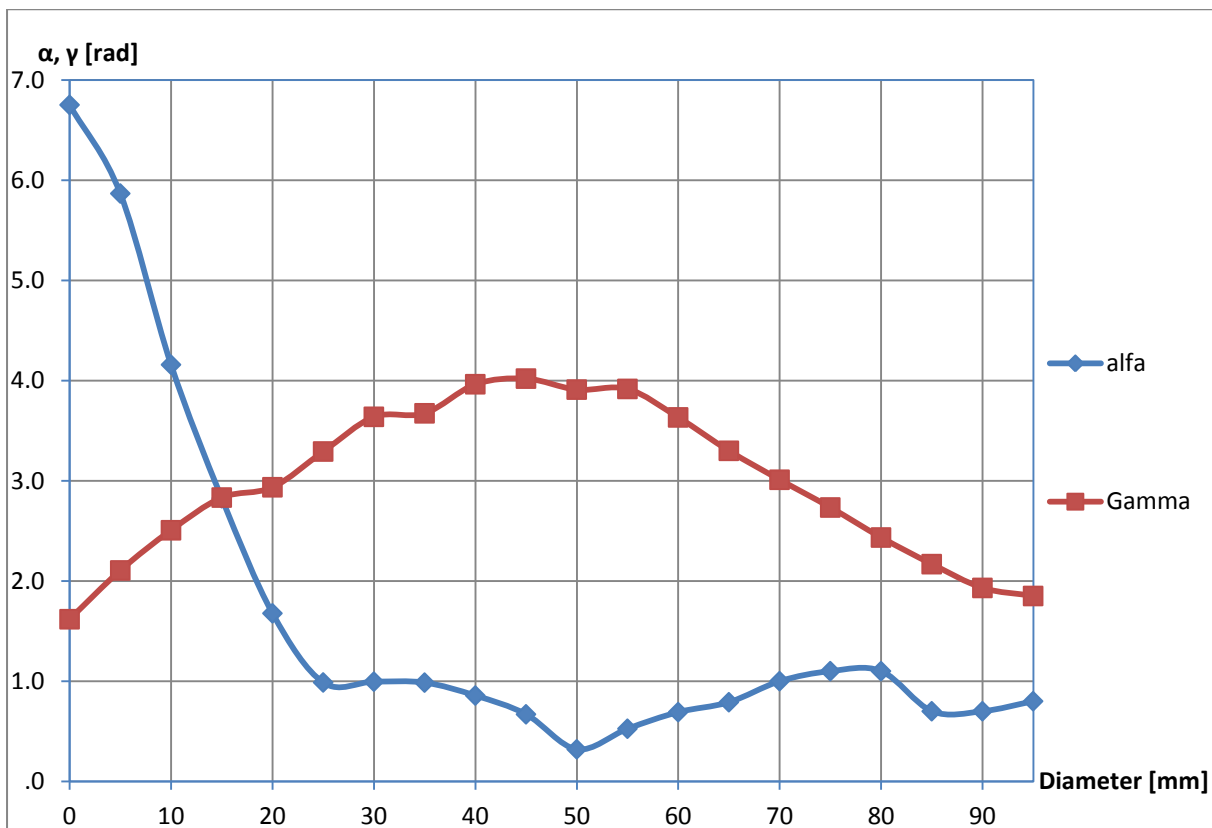


Figure 5.2.1 Flow angle value plotted for the experimental test with maximum Mach number equal to 0.68.

The experimental results confirm that also in this case the flow is not uniform.

Only the experimental results for Mach number equal to 0.68 are plotted, because the results regarding the experiment with Mach number equal to 0.58 presents the same behavior.

6. VALIDATION OF THE RESULTS

6.1 VALIDATION ASSESSMENT PROCESS

Validation is defined as “The process of determining the degree to which a model is an accurate representation of the real world from the perspective of the intended uses of the model”. (AIAA G-077-1998)

Validation has also been described as "solving the right equations". It is not possible to validate the entire CFD code. One can only validate the code for a specific range of applications for which there is experimental data. Thus one validates a model or simulation. Applying the code to flows beyond the region of validity is termed prediction.

Validation examines if the conceptual models, computational models as implemented into the CFD code, and computational simulation agree with real world observations. The strategy is to identify and quantify error and uncertainty through comparison of simulation results with experimental data. The experiment data sets themselves will contain bias errors and random errors which must be properly quantified and documented as part of the data set. The accuracy required in the validation activities is dependent on the application, and so, the validation should be flexible to allow various levels of accuracy.

Each CFD simulation requires verification of the calculation as specified in the discussion of Verification Assessment.

The process for Validation Assessment of a CFD simulation can be summarized as:

- Examine Iterative Convergence. Validation assessment requires that a simulation demonstrates iterative convergence. In the examined case, more steps are performed in

order to assure iterative convergence and so a good quality of the mesh. The first step consisted in doing a simulation with advection scheme Upwind and the convergence criteria was set as max residual target $1 * 10^{-4}$. As know, the advection scheme Upwind is a first order scheme and contains lots of numerical diffusion. This means the flow is damped artificially more than it should be which results in easy and tight convergence, but inaccurate results. For this reason a second simulation is performed with advection scheme High resolution. This scheme uses a second order scheme when possible. It contains far less numerical diffusion. This means the flow has less artificial damping and therefore closer to the correct amount of damping.

- Examine Consistency. One should check for consistency in the CFD solution, for example plotting the value of pressure, velocity and temperature and controlling that are reasonable.
- Examine Spatial (Grid) Convergence. The CFD simulation results should demonstrate spatial convergence.
- Examine Temporal Convergence. The CFD simulation results should demonstrate temporal convergence.
- Compare CFD Results to Experimental Data. Experimental data is the observation of the "real world" in some controlled manner. By comparing the CFD results to experimental data, it's hoped that there is a good agreement, which increases confidence that the physical models and the code represents the "real world" for this class of simulations. However, the experimental data contains some level of error. This is usually related to the complexity of the experiment.
- Examine Model Uncertainties. The physical models in the CFD code contain uncertainties due to a lack of complete understanding or knowledge of the physical processes. One of

the models with the most uncertainty is the turbulence models. As just said, another important uncertainties model regards the geometry of the channel facility. According to the numerical results, one of the most important causes leading the non uniformity flow in the test section is the behavior of the flow in the T-junction. Cause leakage of geometry knowledge, this was in part supposed in our geometry model and so leads to uncertainties.

6.2 FLOW VALIDATION AND DISCUSSION

In the figure 6.2.1 and 6.2.2 the results for the experimental and numerical tests are plotted for the value of mass flow equal to 1.55 respectively for α and γ .

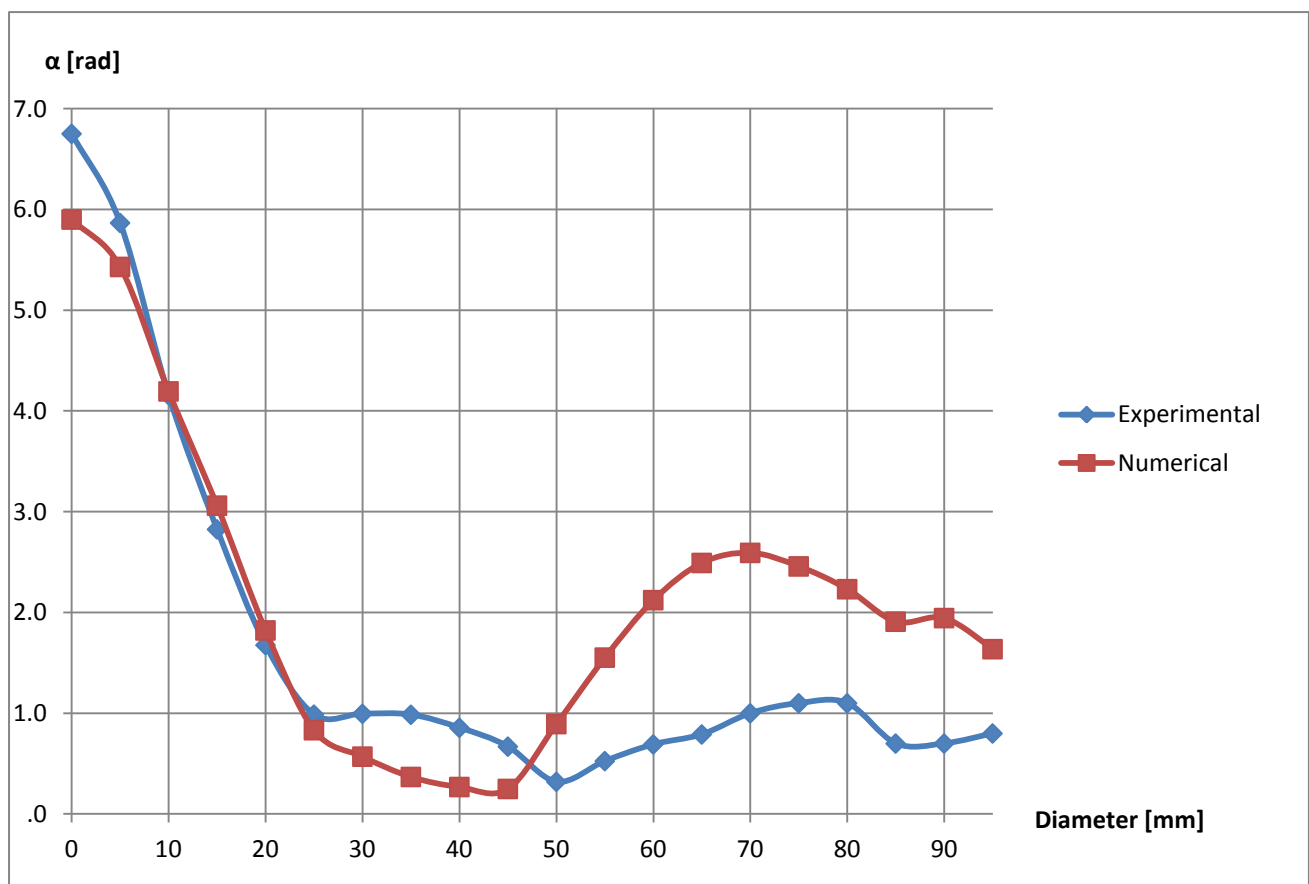


Figure 6.2.1 Flow angle α value plotted for the numerical and experimental test

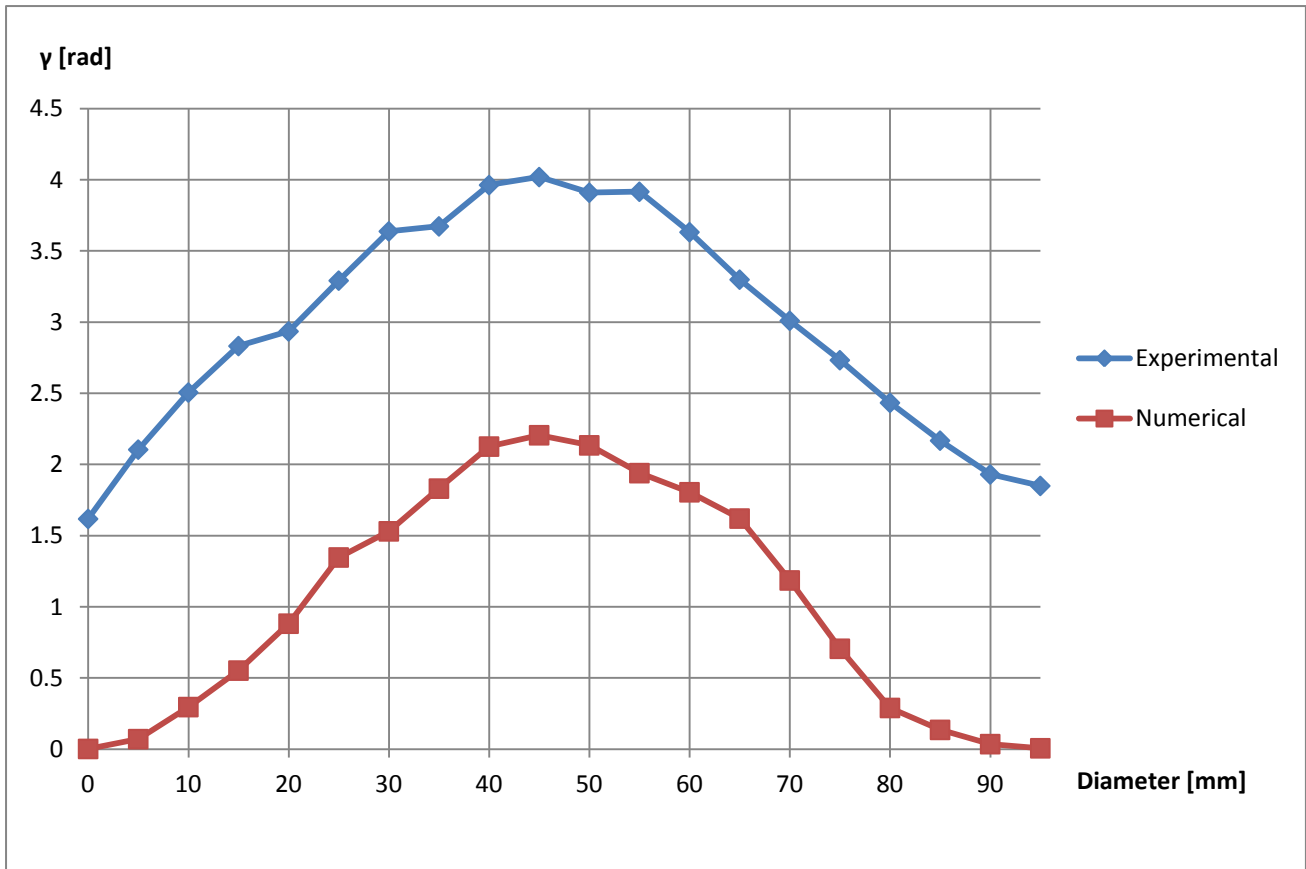


Figure 6.2.2 Flow angle γ value plotted for the numerical and experimental test

The numerical and experimental results for the value of mass flow 1.45 kg/s present the same behavior.

According to the data, the flow cannot be considered validated because the points have too distant values.

Definitely this is affected by the fact that some parts of the numerical geometry are supposed. According to the numerical results, it has been said that the t-junction has an important effect on the streamline curvature and consequently on the uniformity of the flow

in the test section, but as said, the t-junction geometry has been supposed because not enough data were available.

The fact that the flow presents different axial velocity between numerical and experimental data with the same mass flow value cannot be considered so important because the curves present the same behavior for different mass flow applied.

Another important thing can be observed: the experimental and numerical curves have the same trend, this confirms that the flow in the test section is not uniform. This can be easily seen looking at the γ angle plotting, where the curves have an offset of about 1.5 radians and until 50 mm the same trend in the α curves.

For this reason it's suggested in the future to investigate first the real geometry of the t-junction, but the channel facility needs to find a new collocation that allows the pipe before the nozzle to be extended in order to obtain uniform flow in the test section. The actual place where the channel is located doesn't allow this type of work. This is what is principally proposed for the future scope of this thesis.

7. POSSIBLE SOLUTIONS TO UNIFORM THE FLOW

7.1 CHANGING THE NOZZLE GEOMETRY

As described in the numerical results, the nozzle geometry can be improved in order to avoid the adverse pressure gradient at the outlet section of the nozzle. Typically, a contraction design starts with the selection of a contraction ratio (CR), which is mostly dictated by a consideration of the available space. Once the value of CR is determined, the nozzle shape and length must be chosen so as to satisfy predetermined design criteria.

By far, the most direct way for an engineering contraction design is that suggested by Morel. The design of wind tunnel contractions has been based on a pair of cubic polynomials, and the parameter used to optimize the design for a fixed length and contraction ratio, has been the location of the joining point.

The coordinate system for the contraction profile is defined with origin on the tunnel centre line at the contraction inlet plane, and x coordinate increasing in the downstream direction. The y coordinate defines the contraction profile and z is in the spanwise direction. A sixth order polynomial was chosen to define the profile shape:

$$y = ax^6 + bx^5 + cx^4 + dx^3 + ex^2 + fx + g \quad (7.1.1)$$

The chosen profile has 7 parameters (a-g). Five of these are specified by the inlet and outlet height (200mm and 50mm, respectively), zero slope at the inlet and outlet and zero curvature at outlet. This leaves two parameters available for optimization. These are specified by the inlet curvature and the axial position of the point of inflection relative to the contraction length. The conditions already specified directly provide the following constants for the polynomial

$$g = H \quad f = 0 \quad e = \frac{\alpha}{2}$$

Where:

H= inlet height (half diameter)

α = inlet curvature

i= axial location of inflection point

l= length of contraction

The other constants are defined by the equation:

$$Aw = B$$

Where, for $\alpha=0$ for the standard case (with no inlet curvature):

$$A = \begin{bmatrix} 30i^4 & 20i^3 & 12i^2 & 6i \\ l^6 & l^5 & l^4 & l^3 \\ 6l^5 & 5l^4 & 4l^3 & 3l^2 \\ 30l^4 & 20l^3 & 12l^2 & 6l \end{bmatrix} \quad B = \begin{bmatrix} 0 \\ -h \\ 0 \\ 0 \end{bmatrix} \quad C = \begin{bmatrix} a \\ b \\ c \\ d \end{bmatrix}$$

This non linear system is solved using the function fsolver available in Matlab.

The range of variable i, distance to the point of inflection, which gives a sensible, monotonically decreasing curve is 0.4-0.6 l. Using a lower or higher value of i/l, the profile under or overshoots respectively. This was deemed to be impractical for a contraction profile.

After various simulations, the optimize shape ,that allow a monotonically behavior of c_p , was determined using a value of $i=0.4$.

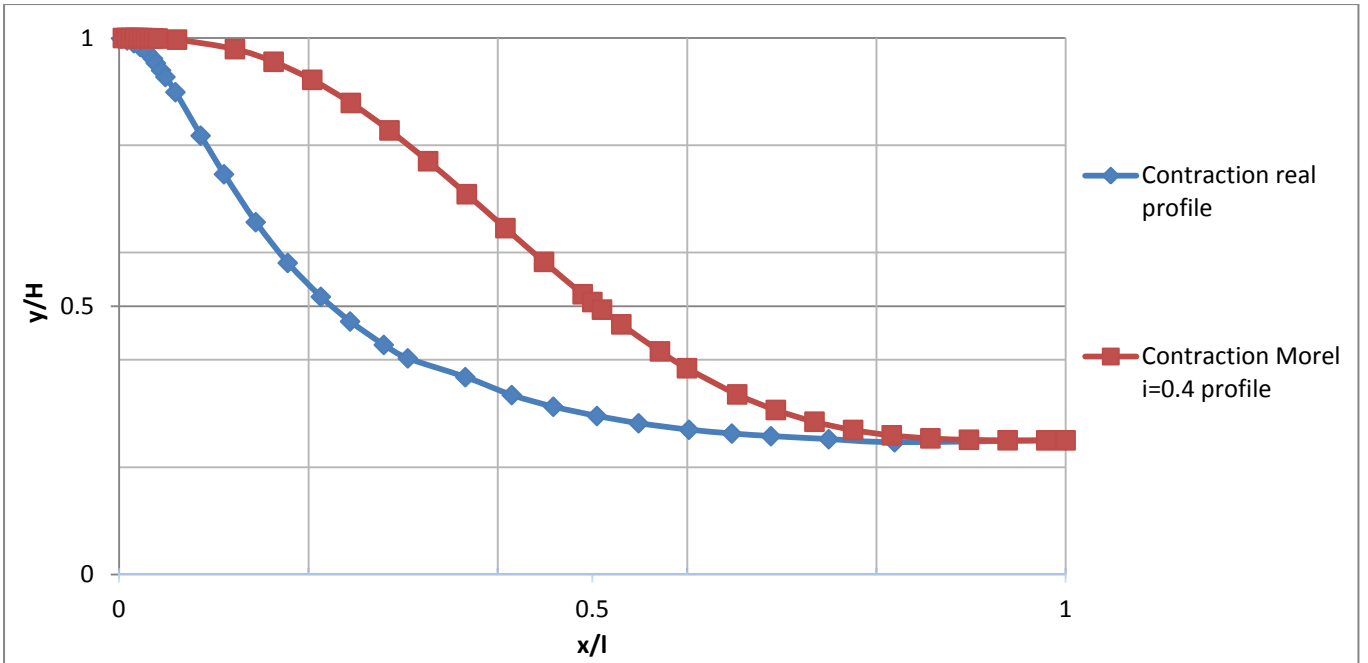


Figure 7.1.1 Schematic of the contractions (half plane)

Consequently, in figure 7.1.2 it's showed the behavior of C_p parameter along the nozzle for mass flow equal to 1.55 kg/s.

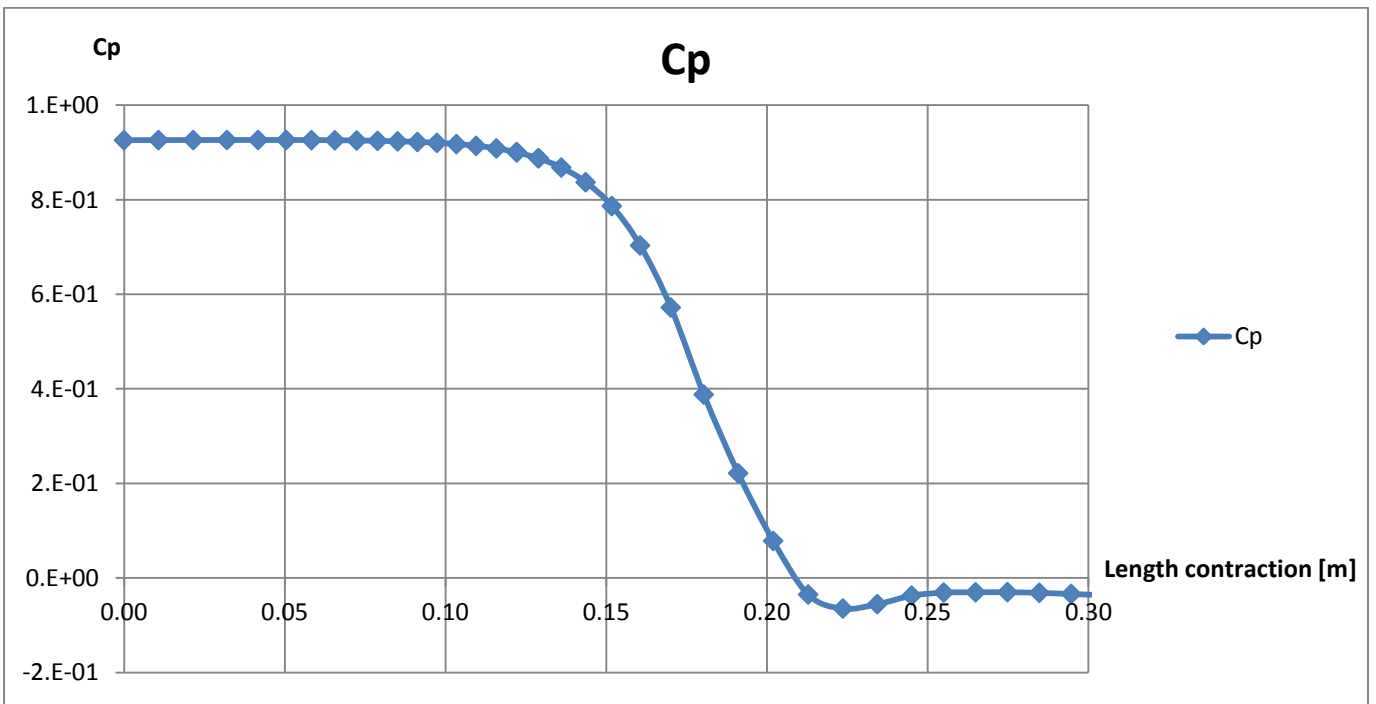


Figure 7.1.2 Cp behaviour in the contraction region of the new nozzle geometry for mass flow 1.55 kg/s

Unfortunately this configuration doesn't allow to achieve reasonable improvements at the no axial velocity components and for this reason it's not suggested to be employed.

7.2 PROVIDE A HONEYCOMB STRUCTURE BEFORE THE NOZZLE

In order to minimize the turbulence and disuniformity before the nozzle, a design structure of honeycomb (such as square, circular and hexagonal cross-section) is implemented using the function submodeling in Cfx-Preprocessor.

Honeycomb is a passage of ducts, laid along the axis of main air stream to suppress the cross velocity components. The cross sectional shapes of honeycombs may be square, circular and regular hexagonal cells, as shown in fig. 7.2.1

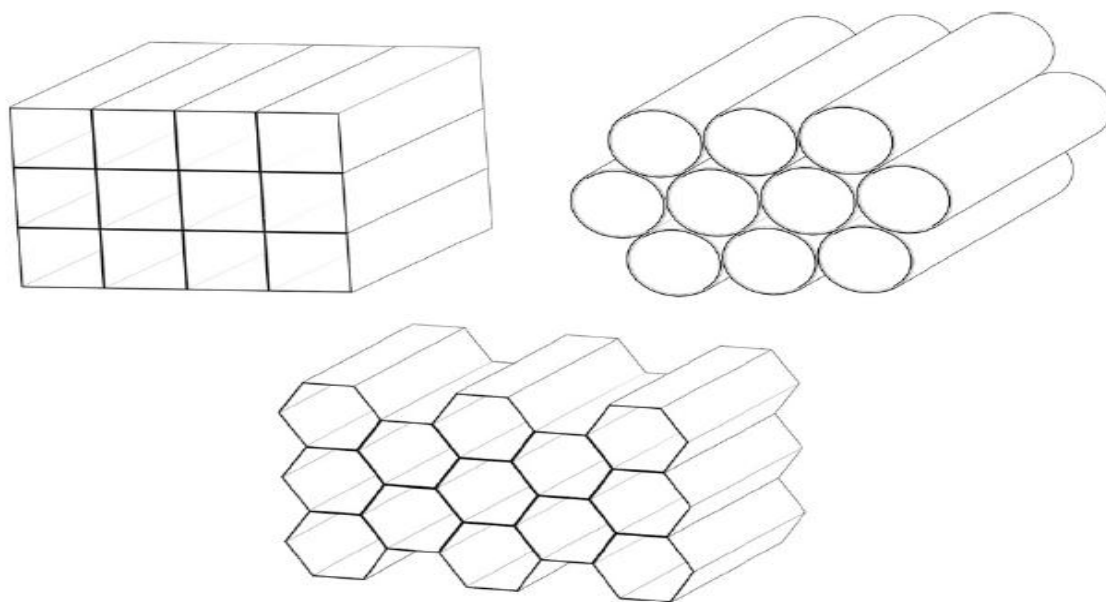


Figure 7.2.1 Schematic of several honeycomb cross-sections including square cell, circular cell and regular hexagonal cell.

The model for honeycomb is meshed always in Icem, a separate fluid region is constructed before the nozzle in the location where loss model is needed.

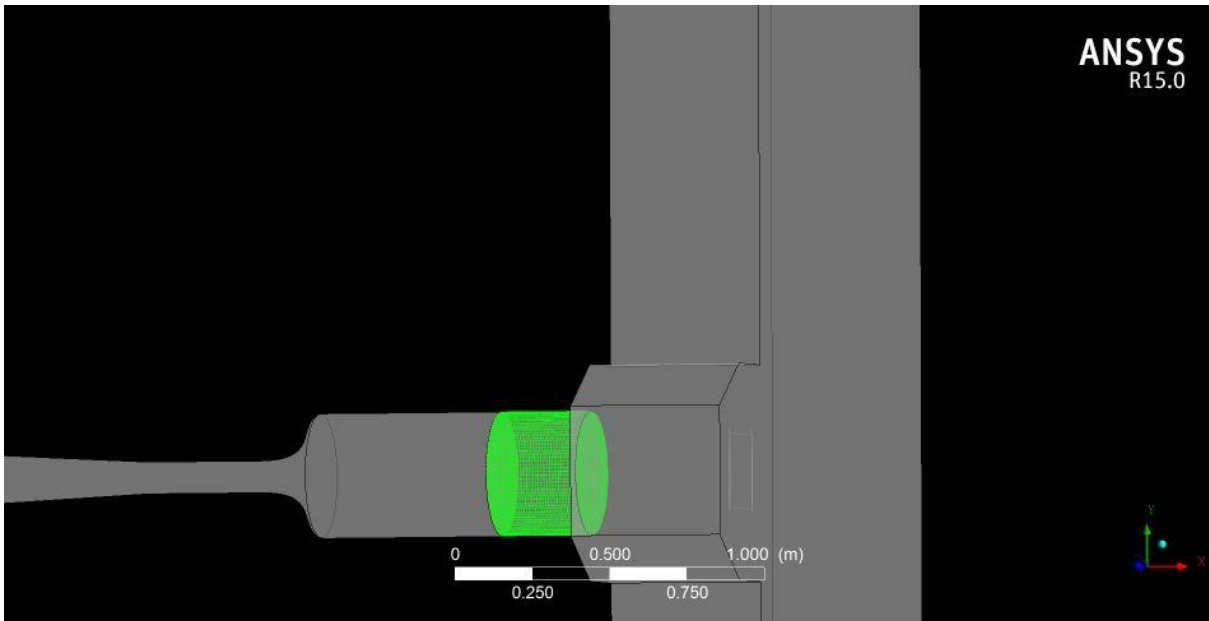


Figure 7.2.2 Fluid region where honeycomb is installed.

Necessary momentum source for an anisotropic porous region of the screen is represented using directional loss model.

Required resistance coefficient for the axial direction is calculated using the equation

$$\zeta = \lambda_1 * \left(3 + \frac{l_0}{d_h} \right) * \left(\frac{F_1}{F_0} \right)^2 + \left(\frac{F_1}{F_0} - 1 \right)^2 \quad (8.2.1)$$

Where F_0 is the total flow area of the honeycomb, F_1 is the cross section area of the front, l_0 is the length of the honeycomb tube, d_h is the hydraulic diameter, λ_1 is the friction coefficient of unit honeycomb depth.

The friction coefficient λ is determined by the following formula

$$\lambda_1 = 0.214 * \Delta^{0.4} \quad (8.2.2)$$

Where Δ is the relative roughness of the honeycomb tubes. This value is assumed 0.0050.

Others assumptions are $\frac{F_1}{F_0} = 2$ and $l_0 = 0.3m$.

The result is for the axial direction $\zeta = 1.39$. For the two transverse directions, a multiplier coefficient of 10 is assumed for the resistance coefficient.

Various investigations are performed at different Mach number value. The results show that honeycomb effectively generates smaller lateral velocity. For example, the simulation regarding mass flow equal to 1.55 kg/s at the compressor, the non axial velocity components at mid working section on vertical plane are plotted in figure 7.2.3. Compared to the axial velocity, the non axial velocity component can be neglect.

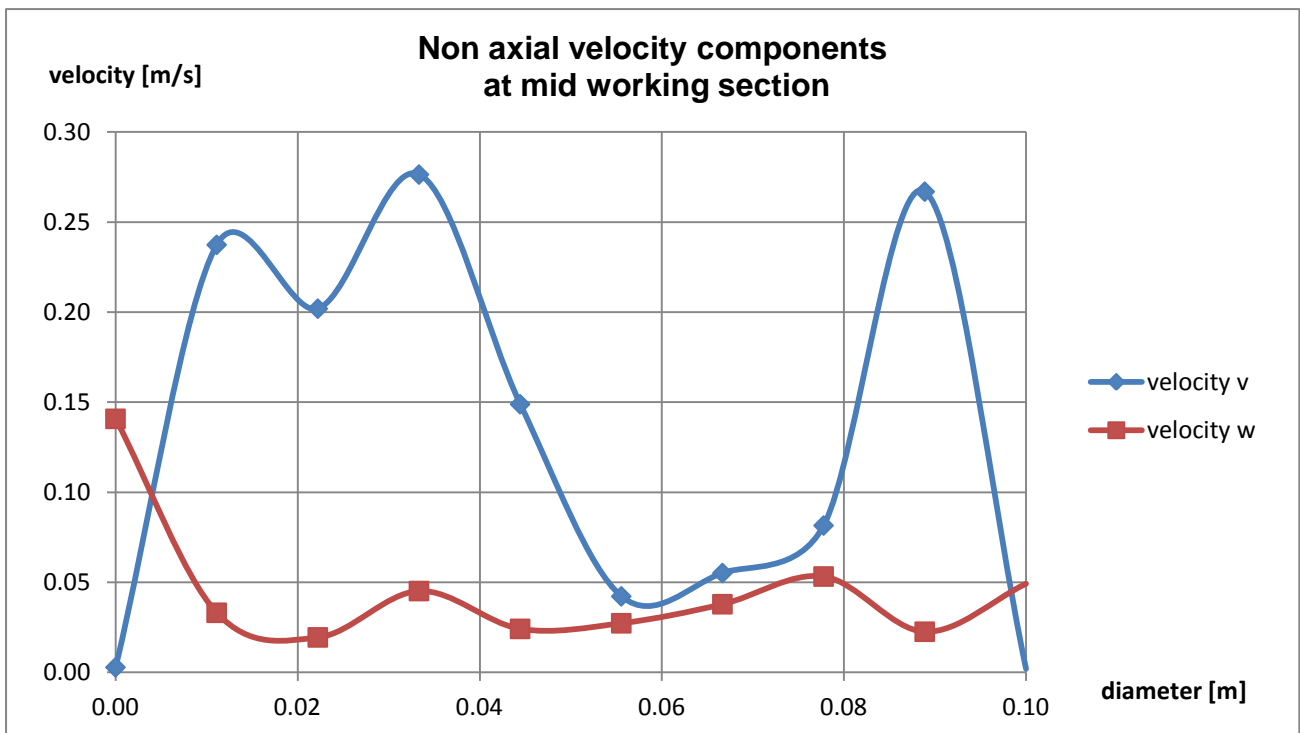


Figure 7.2.3 Variation in lateral velocity at mid working section on vertical plane

8. CONCLUSION

In the turbo machinery department at the University of Duisburg Essen a numerical and experimental investigation in order to discover the velocity profile for a turbulent compressible flow in a channel facility was undertaken. The test section has been located before a diffuser in the pipe that conduits the flow to a compressor.

According to the data, the flow cannot be considered validated because the points have too distant values. Definitely this is affected by the fact that some important parts of the numerical geometry are supposed or no enough data are available about them.

One important thing has been also considered: the experimental and numerical curves have the same trend, this confirm that the flow in the test section is not uniform. This can be easily seen looking at the flow angle plots in the validation results.

For this reason, what is principal propose for the future scope of this thesis it's to investigate first the real geometry of the t-junction and then to find a new collocation that allows the pipe before the nozzle to be extent in order to obtain uniform flow in the test section. The actual place where the channel is located doesn't allow this type of work.

In the case that a new collocation will not be find, a honeycomb structure before the nozzle is suggested. One example of it is reported in the previous chapter using for its modeling the program Icem Ansys.

9. Appendix A. The labVIEW “State machine” Code

The style that has been used for the state machine is the sequence style. This version is used when the order of execution of the tasks to be performed is predefined, and it will always execute from beginning to end in order. In this type of systems, there are a number of distinct steps that need to be performed in a defined order. These steps can be used to create the states in the state machine.

In this case, the following states can be identified: wait, choose new position, wait till new position is arrived, measure the pressure, evaluate data. Once the states have been identified, the enumerated control should be created and each of the above states should be put into.

The enumerated control is wired to the case structure. A shift register is used to save data from and between the different states. The first step is to create the first and default state, called wait. The value of the angle is set to -25° , according the fact that this is the initial point from where the three-hole probe starts to measure. An array of the angle and pressure data has been initialized with a value of 0 and then it will be fill in with the measure collected. This array is necessary in order to plot at the end in a graph the results.

At this point an event occurs and the state “choose new position” is initialized. In this case the angle value of -25° degree is set as Zielposition (objective position), the only movement allowed at the engine is the rotation and absolute reference system is chosen. Everything is inserted in a flat sequence structure in order to don't allow the code to go to the next step without have done all this operations.

The next state is called “Wait till new position is arrived”. The engine has to be launch in order to allow the measurement system to reach the objective position. Another flat

sequence structure is inserted, first the engine is started and after that 200ms are left (sufficient to achieve the objective position) the engine is closed. At this point, the signal “control ready” is on and we can pass to the next state.

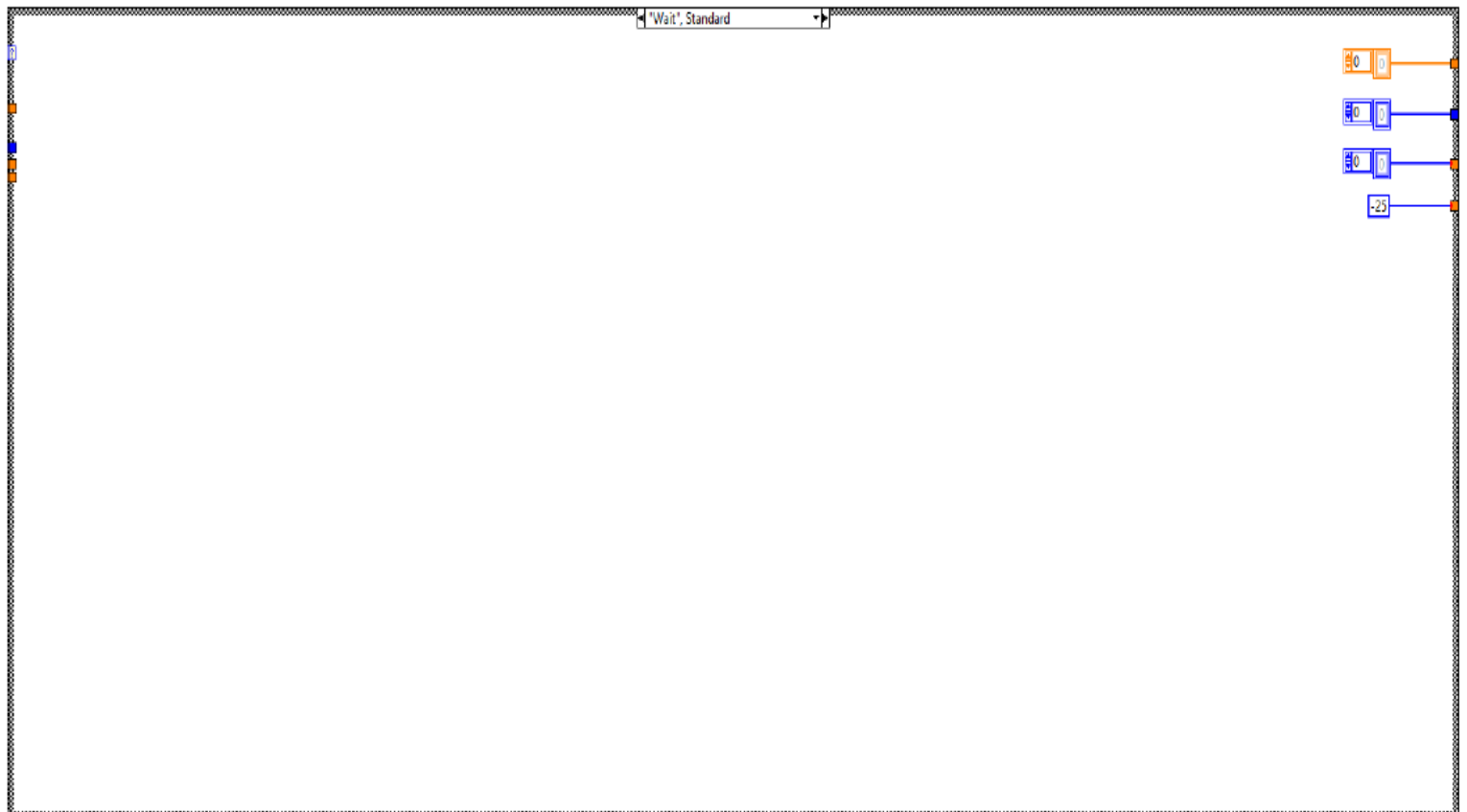
At the state “measure pressure” we enter a case structure, in which the previous steps are done again whether the value of the angle doesn’t reach 26° . The pressure values are continuously saved in the array, taking respectively 20 measures for each angle and doing a mean of it in order to improve the precision. When the three hole probe achieves 26° degrees, the data can be compared and we can pass to the state “evaluate data”. At the state “evaluate data” the data collected are plotted in a graph, where along the x axis there are the angle values and along the y axis the pressure static values respectively. In order to have a comprehensible graph, a polynomial line is also plotted to connect the points obtained.

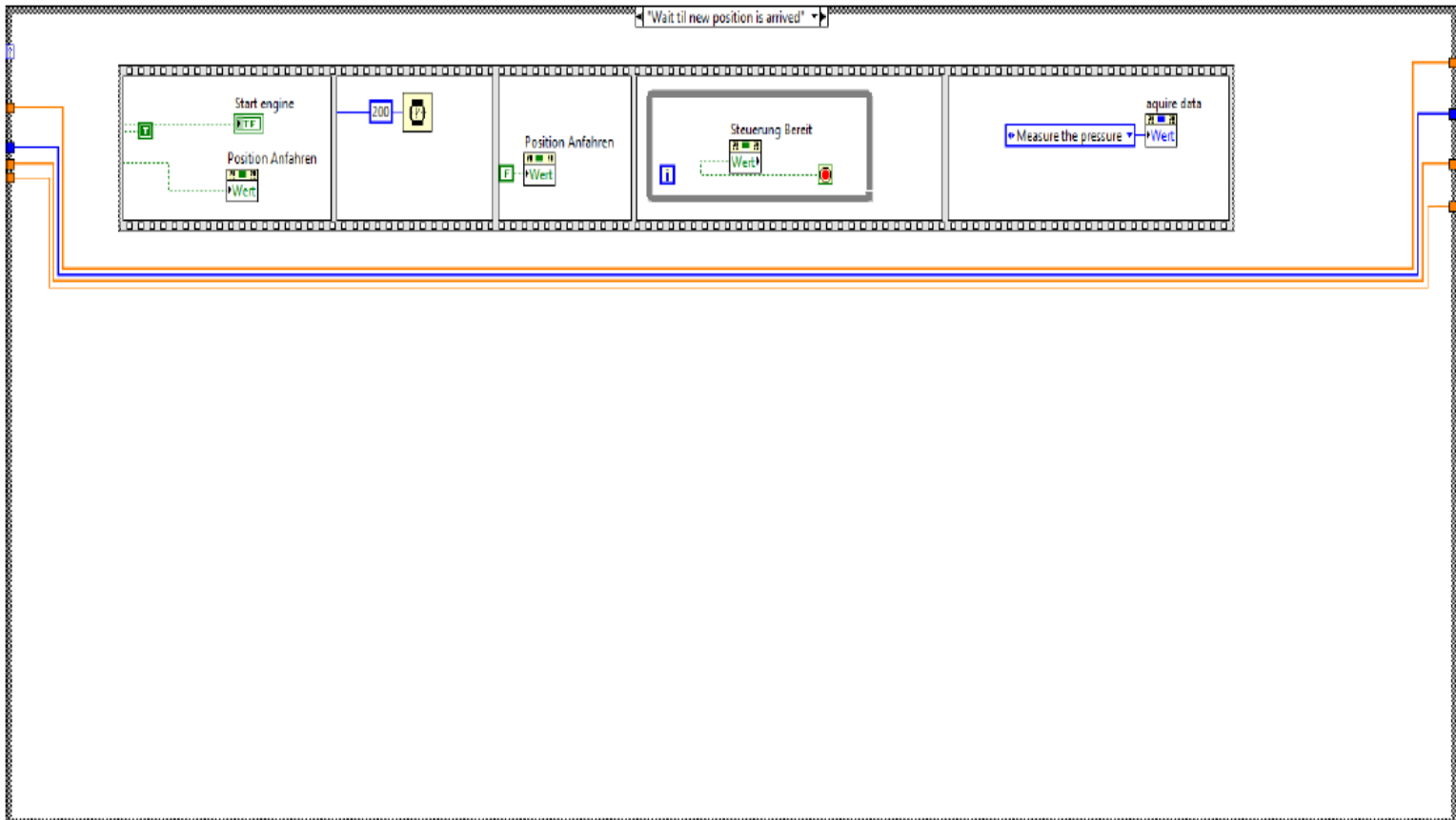
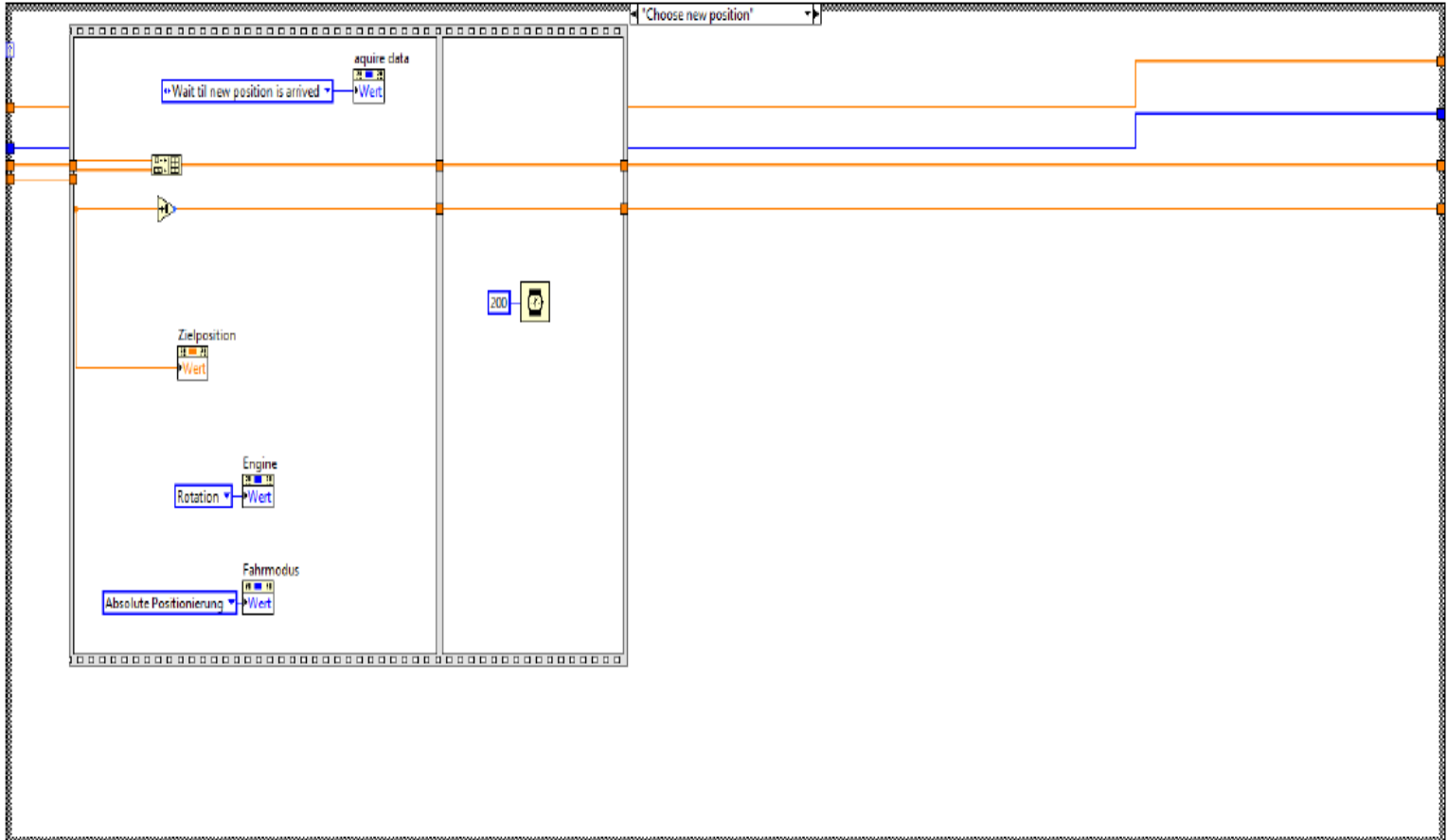
As told before, when the instrument measures the smallest value of static pressure, this is the correct angle in which the velocity measures have to be taken.

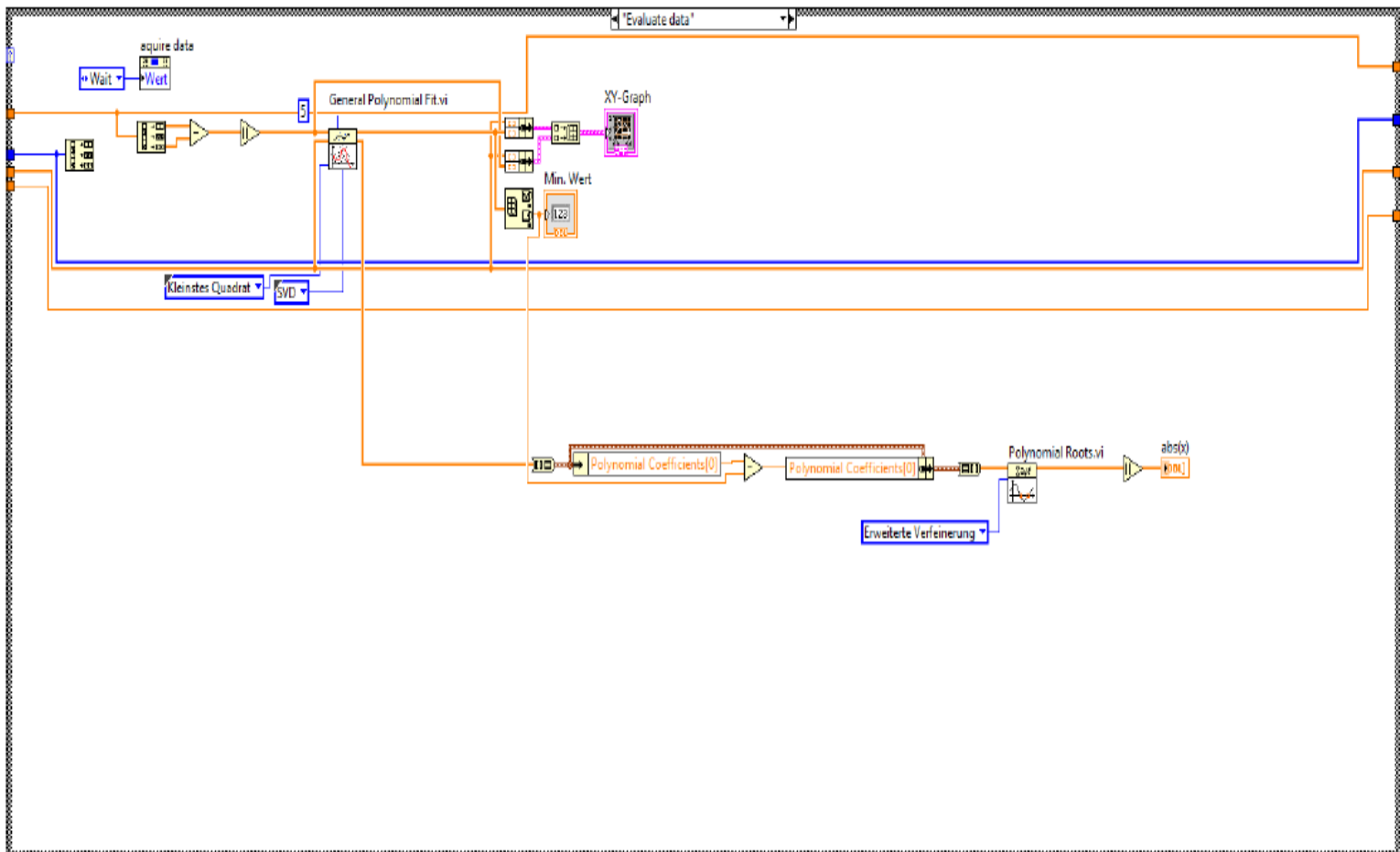
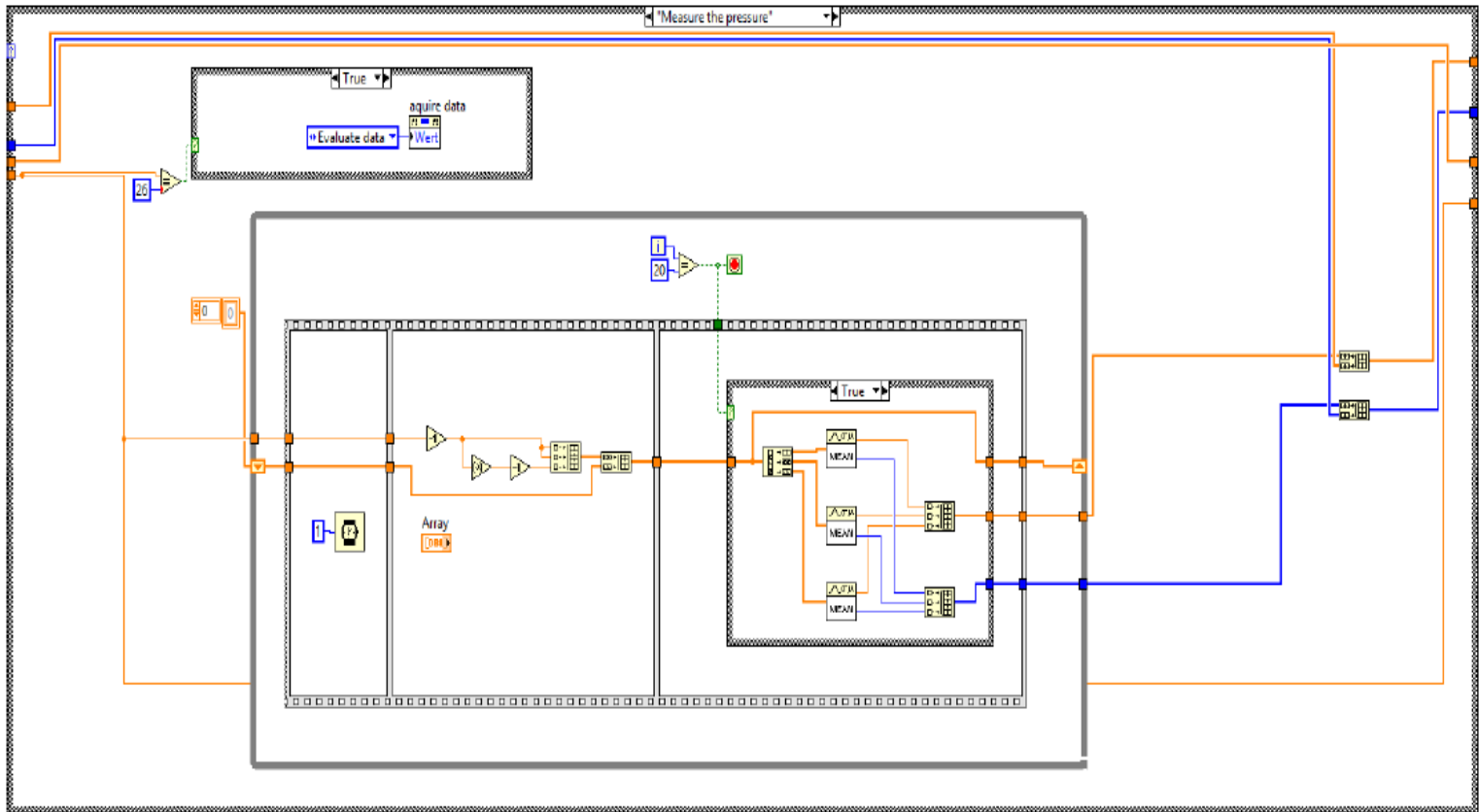
In order to obtain the velocities data, a last code has been done, where the temperature, static and total pressure measures for every angle are taken. According to the equation 4.1.3, the velocity can be calculated and the data can be written in a text file.

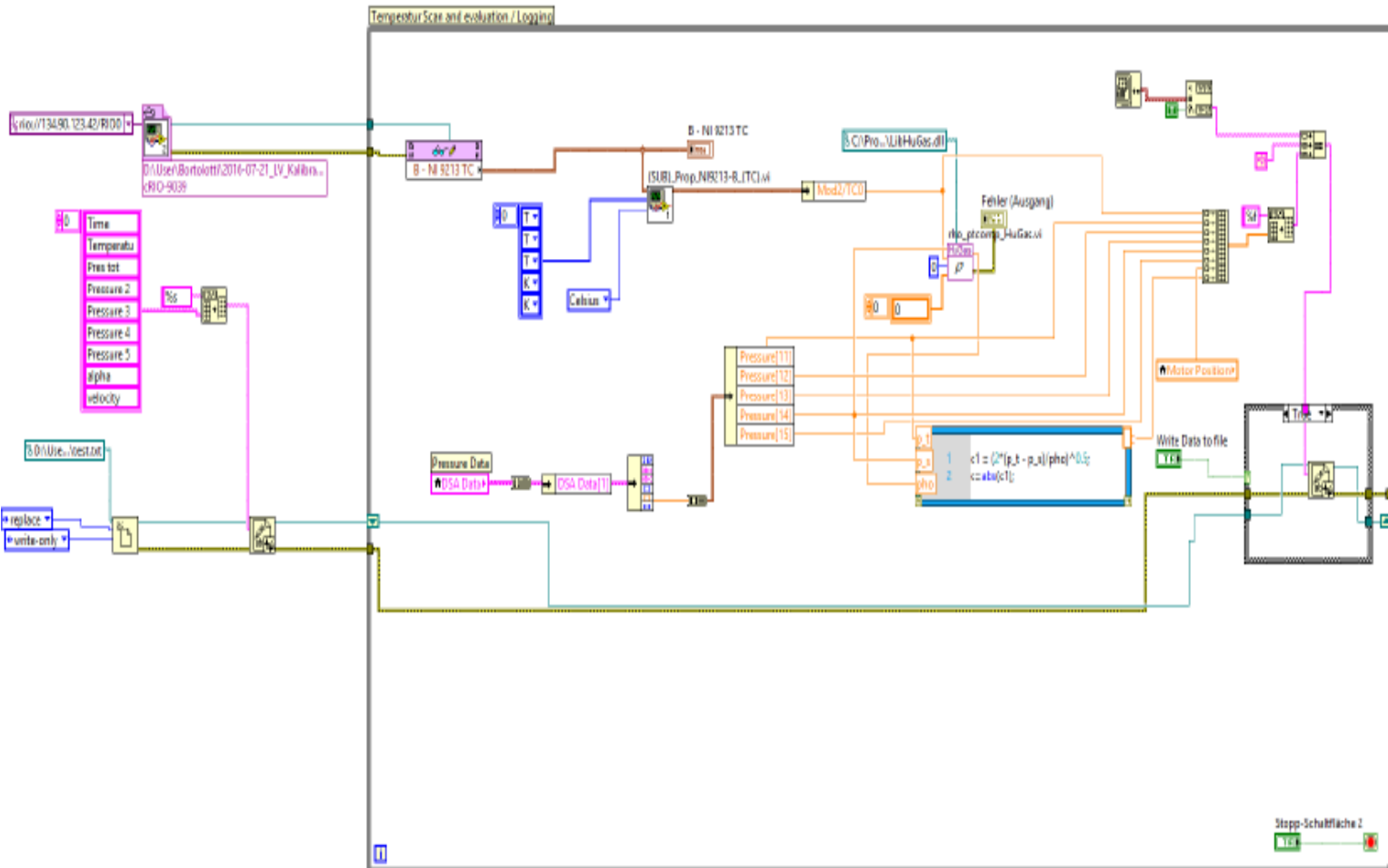
Software interface for DSA (Dose Rate) measurement and control. The interface is divided into several functional areas:

- Top Left:** "square data" section with a "Wait" button and a "Min. Wert" (Minimum Value) display showing 0. Below it is a "Start engine" indicator.
- Top Center:** "registrierte" (Registered) section with "Pressure Scan" and "Traversing" tabs. It contains a grid of buttons for "Connect" and "Disconnect" for DSA 3217 - A and DSA 3217 - B. Below this is the "Physikalische Einheit" (Physical Unit) set to "ZERO Korrektur" and "DSA-Steuerung" (DSA Control) with buttons for "KEINE Korrektur", "Standby", and "Stopp DSA".
- Top Right:** "DSA Data" section with a "Frame #", "Time", "Time Units", "Channel", "Pressure", and "Temperature" display area.
- Middle Left:** "Array" section with a vertical stack of input fields.
- Middle Center:** "XV-Graph" (X-ray Graph) showing "Amplitude" vs "Zeit" (Time). The graph shows a flat line at 0 amplitude over a time range from -5 to 5.
- Middle Right:** "DSA Befehle" (DSA Commands) section with a "Befehl(e) senden" (Send Command(s)) button and "Antwort DSA-A" / "Antwort DSA-B" (Response DSA-A / B) text areas.
- Bottom Left:** "Fehler (Ausgang)" (Error (Output)) section with a "Status" (0) and "Code" (0) display, and a "Quelle" (Source) list.
- Bottom Center:** "Fehler Aus" (Error Out) section with a "Status" (0) and "Code" (0) display, and a "Quelle" (Source) list.
- Bottom Right:** A vertical list of "Mod/TC" (Module/Thermocouple) status indicators for TC0 through TC15, each showing a value of 0.00000000.









REFERENCES

H K Versteeg, W Malalasekera, "An introduction to computational fluid dynamics", second edition, Person Education Limited 2007

A.J. Ward-Smith, "The fluid dynamics of flow in pipes and ducts", Clarendon press Oxford 1980

Ismail B. Celik, Urmila Ghia, Patrick J. Roache, " Procedure for estimation and reporting of uncertainty due to discretization in CFD application", Journal of fluids engineering

Ansys Inc., "Ansys ICEM CFD Tutorial Manual", 2012

Manshadi M., Mirzaei M., Soltani M.R. and Ghorbanian K., "Control of pressure gradient in the contraction of a wind tunnel", International Journal of Mechanical, Aerospace, Industrial, Mechatronic and Manufacturing Engineering, 2008

Gary W. Johnson, "LabVIEW Graphical programming", McGraw-Hill, 1997